Scientific Research Publishing

Open Journal of Applied Sciences, 2026, 16(4), 1413-1449
https://www.scirp.org/journal/ojapps
ISSN Online: 2165-3925
ISSN Print: 2165-3917

Study of the Modeling and Evaluation of the Electromagnetic Radiation Rate of GSM Base Station Antennas in a Given Geographic Area Using the Metric Method

Anthony Bassesuka Sandoka Nzao[1*], Emmanuel Moke Aman[2]

[1]Department of Electrical Engineering, ISTA Kinshasa, Kinshasa, Democratic Republic of the Congo
[2]Department of Electrical Engineering, and Telecommunications Option, ISTA Kinshasa Doctoral School, Kinshasa, Democratic Republic of the Congo
Email: *bass_sandoka@yahoo.fr

How to cite this paper: Nzao, A.B.S. and Aman, E.M. (2026) Study of the Modeling and Evaluation of the Electromagnetic Radiation Rate of GSM Base Station Antennas in a Given Geographic Area Using the Metric Method. *Open Journal of Applied Sciences*, **16**, 1413-1449.
https://doi.org/10.4236/ojapps.2026.164082

Received: February 20, 2026
Accepted: April 27, 2026
Published: April 30, 2026

Abstract

The widespread deployment of GSM mobile networks has led to a significant increase in the number of base station antennas, raising growing concerns about public exposure to electromagnetic fields (EMF). This study aims to model and assess the electromagnetic radiation levels emitted by these antennas in a specific geographic area, using a combined modeling and measurement approach based on the metric method. The methodology relies on field data collection, mathematical modeling of the electromagnetic field, and analysis of measured exposure levels. The results are compared to current international standards, allowing for the assessment of installation compliance and the identification of potentially high-exposure areas. This study contributes to a better understanding of the impact of GSM antennas on public health and offers insights for optimizing the deployment of telecommunications infrastructure. The results, obtained through 2D and 3D measurements and simulations, demonstrate that the tools and approaches used are effective for analyzing electromagnetic exposure in complex environments.

Keywords

Electromagnetic Radiation, GSM Antennas, Modeling, Metric Method, Okumura-Hata Empirical Model, Human Exposure, Formatting

1. Introduction

The massive deployment of GSM mobile phone networks has led to an exponen-

tial increase in the number of base station antennas, raising concerns about public exposure to electromagnetic fields (EMFs) emitted by these infrastructures [1]-[4]. The issue of the effects of EMFs on human health is well documented, with extensive research on the interactions between electromagnetic waves and biological matter [5]-[7]. The thermal effects of EMFs, particularly the heating of biological tissues, are widely established, while non-thermal effects, especially at low doses, remain a subject of scientific debate [8]-[10]. International standards, such as the Specific Absorption Rate (SAR), define exposure limits, but accurately assessing radiation levels in complex environments, taking into account topography and buildings, remains a major challenge [11]-[13].

Despite the existence of these regulations, there is a lack of precise data on the spatial distribution of electromagnetic radiation levels in specific geographic areas, taking into account the variability of urban density and topography [14]-[16]. This gap makes it difficult to accurately assess health and environmental risks, as well as to optimize networks to minimize exposure while ensuring quality of service [17]-[19].

The objective of this study is to model and evaluate the levels of electromagnetic radiation emitted by GSM base station antennas in a defined geographical area, combining field measurement and mathematical modeling approaches. The tools used include electromagnetic field modeling based on Hertzian dipole theory [17] [18], as well as the empirical Okumura-Hata model for analyzing measured and simulated exposure levels. Given the growing concern regarding human and environmental exposure, this study seeks to accurately characterize exposure levels (SAR) and propose strategies for optimizing antenna placement, using an integrated methodology combining 3D numerical simulations and in situ measurements [19].

The main assumptions used in this study are as follows: the metric method, combining theoretical modeling and mapping of emission sources, allows for reliable estimates of EMF levels in a given area. It is expected that the variation in radiation levels will be significantly influenced by factors such as distance from antennas, antenna power, and local environmental factors (topography, buildings, urban structures). Accurate mapping of electromagnetic radiation will make it possible to identify areas of high exposure requiring adjustments to antenna placement.

This study is based on the collection of field data relating to the characteristics of GSM antennas (power, height, tilt), the creation of a 3D digital model of the studied geographical area (terrain and infrastructure), and the modeling of electromagnetic fields using advanced simulation software. The study continues with the generation of power density maps (W/m^2) and SAR maps, followed by a comparison of the simulated results with measurements taken in the field using a spectrum analyzer to validate the reliability of the model.

We assumed that the average peak values of the measurements take into account the contribution of all sites within our sample.

The tools used for the various measurements provide direct results for the E

and S parameters in specific units (V/m and W/m^2) without requiring intermediate calculations.

2. Methods

2.1. Technical Description of a GSM Relay Site

2.1.1. General Consideration

A GSM (Global System for Mobile communications) relay site is an infrastructure comprising a base station (BTS) [20]-[23] with its antennas, a tower, a technical shelter for equipment, an air conditioning system, power systems (batteries, generator) and transmission links to the core network [24] [25], managing the coverage of a radio cell for mobile communication, with an architecture that also includes BSCs (base station controllers) and the MSC (switching center) [26] [27].

2.1.2. Physical and Technical Elements, Operation, and Network Architecture

According to information from the literature [28]-[30], the physical and technical elements of a GSM relay site are as follows:

- Pylon/Mast: Metal structure (guyed or self-supporting) supporting the antennas at an optimal height for radio coverage.
- Antennas: Transmit and receive radio signals (frequencies such as 900 MHz, 1800 MHz) to and from mobile devices.
- BTS (Base Transceiver Station): The electronic heart of the site, managing radio communication with mobile devices, composed of several TRX (transceivers).
- Technical shelter (Shelter): Container housing electronic equipment (BTS, power supplies, batteries, air conditioning).
- Air conditioning system: Maintains a stable temperature for the proper functioning of sensitive equipment.
- Power supply: Ensures continuous operation with backup batteries and often a generator.
- Grounding & protection: Overvoltage and discharge protection systems (lightning rods).
- Transmission links: Connection of the site to the central network (fiber optic, microwave link).

According to the work proposed by [31]-[34], such a system has the following operations and architecture:

- Cell: Geographic area covered by a base station (BTS).
- BSC (Base Station Controller): Controls several BTS, manages radio resources and call transfers (handovers) between cells.
- MSC (Mobile Switching Center): A switching center that manages calls, authenticates users and connects them to the fixed network or other networks.
- Radio dialogue: The mobile connects to the BTS, which transmits the information to the BSC, then to the MSC to route the call, with appropriate fre-

quencies and power.

- Authentication: The MSC queries databases (HLR/VLR) to verify the subscriber via the SIM card.
- To achieve this [34]-[36], the key technical indicators of a GSM relay antenna are:
- Frequencies: GSM bands 900 MHz, 1800 MHz, etc.
- Initial speed: 9.6 kbps (GSM 2G), evolving towards higher speeds with GPRS, EDGE.
- Frame structure: 8 time slots per channel to multiplex users.

A telecommunications site, also known as a GSM site, is a location where a telecommunications operator has installed equipment to form part of its network, thereby providing a range of services to populations living within a certain radius of the site. This location may be shared with other operators [37]. It is characterised by its configuration, which is linked to its urban environment, and by the infrastructure put in place by one or more mobile operators [38]. Open, elevated locations are preferentially chosen to allow for optimal signal propagation and an optimised network [39]. Depending on the situation, this is achieved either by using a metal support structure (pylon) or by utilising an existing building in the surrounding area [40].

Besides the supporting structure, a telecommunications site primarily comprises the following elements, schematically represented in **Figures 1-2** [40].

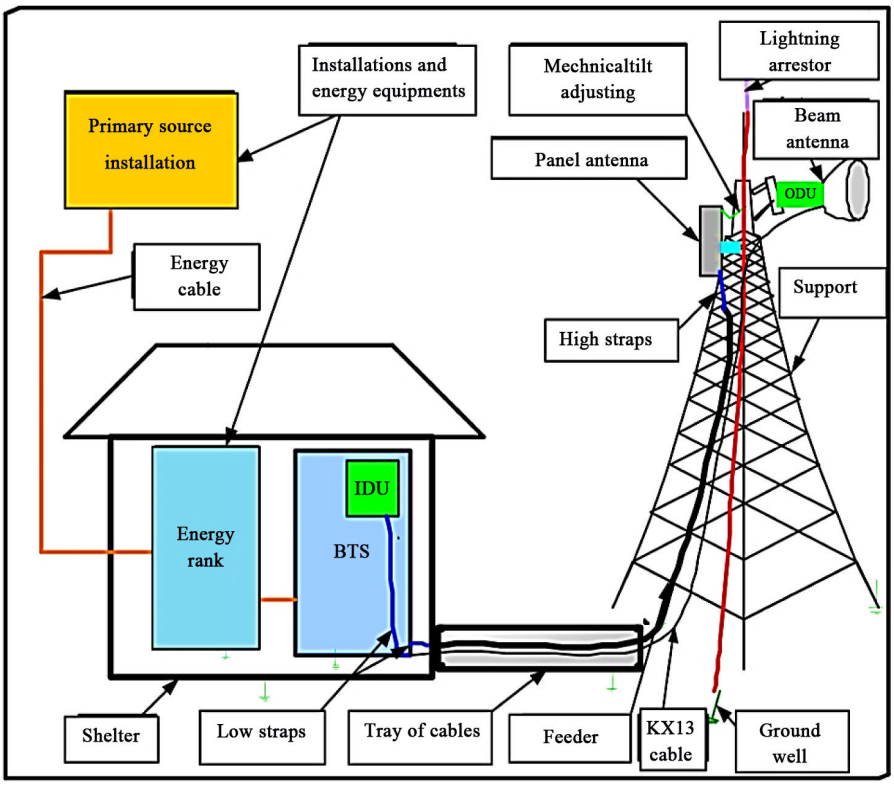

Figure 1. Composition of a GSM site [40].

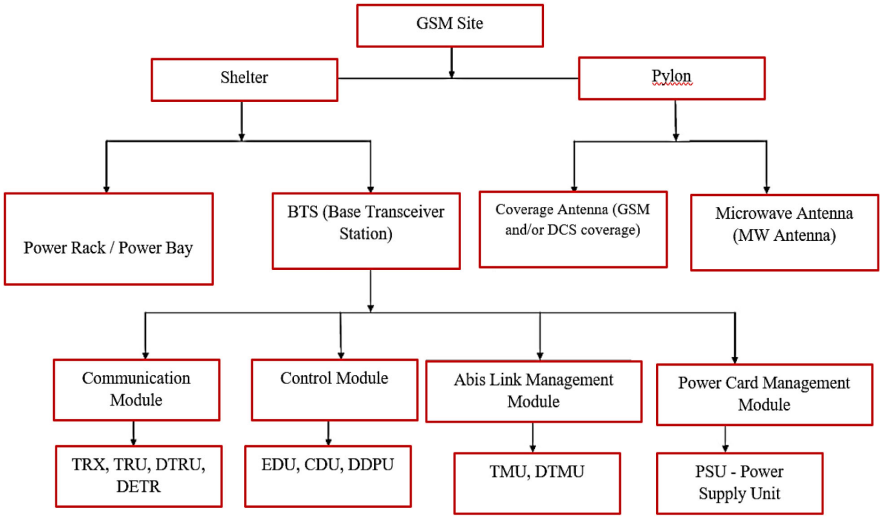

Figure 2. Detailed description of the elements present in a GSM site [41].

2.1.3. GSM Antennas and Essential Characteristics

An antenna is a system that converts electrical energy into electromagnetic energy for reception and transmission. Several criteria are used to describe the characteristics and performance of antennas, such as input impedance, reflection coefficient, directivity, gain, and radiation patterns.

The antenna has multiple roles, the main ones being:

- To allow for a proper adaptation between the radio system and the propagation medium.
- To ensure the propagation or reception of energy in preferred directions.
- To transmit information in the most perfectly feasible way. Furthermore, to present the performance of antennas, several criteria are used [20] [23].

These criteria are classified into two groups. The first group characterizes the antenna as an electrical circuit component with an input impedance and a reflection coefficient (Z_{in} and S_1), and the other group shows great interest in its radiation characteristics, such as the radiation pattern, directivity, and gain.

Finally, it should be noted that the concept of power (absorbed or radiated) is essential to the study of antennas. An antenna is characterized by various factors that can be ordered either into electrical characteristics or into technical radiation specifications.

2.1.4. Principle of Electromagnetic Radiation from GSM Antennas

According to wave theory, all electromagnetic radiation possesses fundamental properties and behaves predictably [42]. Electromagnetic radiation is composed of an electric field (E) and a magnetic field (H). This radiation can be intentional, as is the case for antennas that emit EM energy to establish wireless communication with radio receivers, or unintentional, as with conductors carrying electrical energy. The electric field varies in magnitude and is oriented perpendicular to the direction of radiation propagation (**Figure 3**).

The magnetic field is oriented perpendicular to the electric field. Both fields

travel at the speed of light (c). The radiation is characterised by several parameters, including the radiation pattern, radiated power, directivity, gain, radiation resistance, polarisation, bandwidth, and quality factor [43].

These parameters are respectively modeled by expressions 1 - 10.

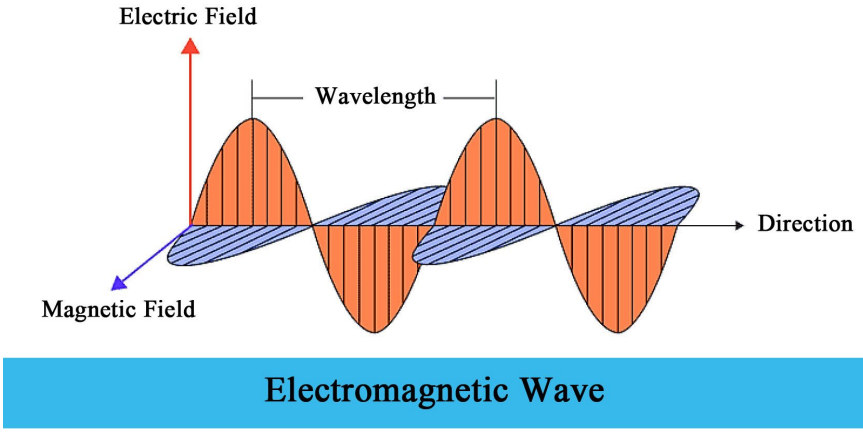

Figure 3. Plane electromagnetic wave [44].

The radiated field at long distances is a function of θ (Site angle: vertical plane) and ϕ (Azimuth angle: horizontal plane). It can therefore be written, up to a factor, in the form:

$$E(\theta,\phi) \approx F(\theta,\phi) \tag{1}$$

Or $F(\theta,\phi)$ is called the characteristic function of radiation.

The radiation pattern represents the radiation intensity $K(\theta, \theta)$ as defined later, based on the deflection angles (θ, θ) in space. This representation provides us with the antenna's most efficient radiation directions.

Radiated power is the power that passes through a sphere of infinite radius. It is determined by integrating the Poynting vector over a spherical surface. The Poynting vector in the radiation zone is defined by:

$$\boldsymbol{P} = \frac{1}{2} R_e (\boldsymbol{E} \times \boldsymbol{H}) \tag{2}$$

The power radiated through a sphere of infinite radius is given by:

$$W = \lim_{r\to\infty} \int \boldsymbol{n} \cdot \boldsymbol{P} \mathrm{d}s \tag{3}$$

With n being a normal vector to any point on the surface of the sphere. The radiation intensity is given by the expression:

$$K(\theta,\phi) = \frac{\mathrm{d}W}{\mathrm{d}\Omega} \tag{4}$$

With dΩ, the unit of solid angle. The total radiated power is defined by:

$$W = \int_0^{\pi} \int_0^{2\pi} K(\theta,\phi) \mathrm{d}\Omega \tag{5}$$

The directivity of an antenna characterizes how that antenna concentrates its radiation in certain directions in space. Directivity is the quotient of the radiation

intensity in a direction $\Delta(\theta,\phi)$ by the average value of this radiation intensity for all directions in space.

$$D = \frac{K(\theta,\phi)}{\frac{1}{4\pi}\iint K(\theta,\phi)\,\mathrm{d}\Omega} \tag{6}$$

An isotropic antenna radiates the same power density uniformly regardless of direction. Gain is a quantity that describes the performance of an antenna. The gain of an isotropic antenna is taken as a unit reference (0 dB).

The gain of an antenna in a given direction is the ratio of the radiated intensity to that of an isotropic antenna.

$$G = 4\pi \cdot \left(\frac{\text{Intensite de rayonnement}}{\text{Puissance total en entree}}\right) = 4\pi \cdot \frac{U(\theta,\phi)}{P_{IN}} \tag{7}$$

The direction of maximum radiation is often taken as the direction for deducing the power gain. If η is the radiation efficiency of an antenna, then $P_{IN} = \mu P_{rad}$, where P_{rad} is the total radiated power. The gain is thus written as:

$$G = 4\pi \cdot \eta\left(\frac{U(\theta,\phi)}{P_{rad}}\right) = \eta D(\theta,\phi) \tag{8}$$

The gain is associated with an equivalent radiation area S_r in the direction $\boldsymbol{u}$ defined by relation (9).

These rules are equally valid for Wi-Fi and ISM.

$$G = 4\pi \cdot \frac{S_r}{\lambda^2} \tag{9}$$

Let P_r be the active power radiated by an antenna. If it is possible to know the current I_Q at a point Q of this antenna, we define the radiation resistance at this point with respect to:

$$R_Q = \frac{2P_r}{I_Q^2} \tag{10}$$

2.2. EMC Concept in Telecommunications

Electromagnetic compatibility (EMC) is defined as the discipline that deals with the problems of electromagnetic coexistence of electrical equipment located in the same environment [42]. This is to ensure the proper functioning of this equipment without producing disturbances that could disrupt the normal operation of other nearby electrical devices. In EMC terminology, a system is said to be compatible if, on the one hand, it does not generate excessive disturbances in its environment, and on the other hand, if it is able to function correctly in the presence of nearby disturbances.

This definition leads to two EMC concepts, immunity and emissivity (**Figure 4**), which are associated with conducted and radiated interference. The distinction between these two modes is made according to the transmission medium, which is either the electrical conductor or the ambient air [43].

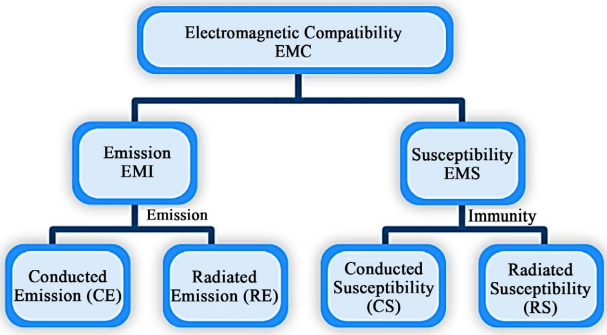

Figure 4. Concepts of EMC [41]-[43].

According to existing literature [43]-[46], the concept of Electromagnetic Compatibility (EMC) in telecommunications, especially with GSM antennas, concerns the ability of a device to function well in its electromagnetic environment without disturbing others, and vice versa, via radio frequency (RF) waves, governing good mobile-antenna link, the management of disturbances (noise, interference) and health risks, notably through the control of the transmission power of antennas and phones to minimize exposure to non-ionizing electromagnetic fields (EMC).

EMC in the GSM context is crucial to guarantee quality of service (no interruptions, good throughput) while managing exposure to waves, using engineering techniques (antennas, power) and respecting regulatory thresholds to minimize nuisances on the network and on health [47].

3. Modeling the Propagation of EM Waves from GSM Antennas

According to the work proposed by [42]-[44], the tools for characterizing the propagation of electromagnetic waves from GSM antennas differ depending on the propagation zone considered because the electromagnetic wave does not have the same propagation properties throughout the space surrounding a source [43]. Depending on the distance from the transmitting antenna, four propagation zones are classically distinguished as shown in the following **Figure 5** [42] [43]: The near field can be divided into two regions, the reactive near field and the radiating near field.

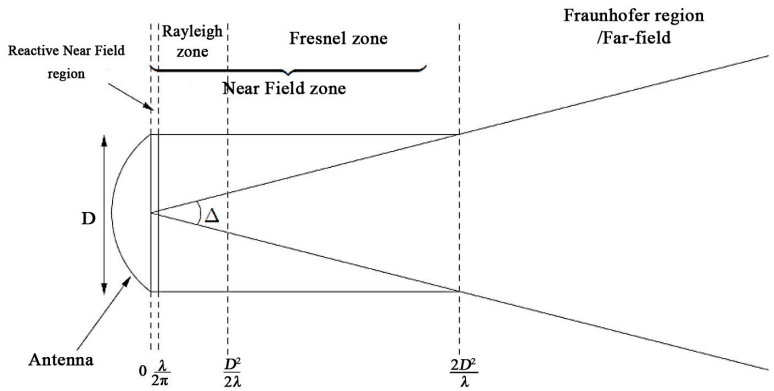

Figure 5. Four radiation zones around a transmitting antenna [42] [43].

Considering [44] the source-receiver distances and in view of the interesting exposure situations that can be studied in a given area (for example the study of the exposure of the facades (receivers) of a school due to a base station (source) located on top of a building opposite or the exposure of the streets of a city due to the base stations located in the area), we naturally place ourselves in the far field zone [44] [45].

Several numerical methods exist for modeling the propagation of electromagnetic waves [45] [46]. Depending on the needs and objectives, some models may be more suitable than others; these include the Hertzian dipole method and numerical methods, particularly the FDTD model [45]-[48]. Before choosing the method to apply for modeling the propagation of EM waves from GSM base station antennas, we first review the fundamental concepts of electromagnetism [47].

3.1. Electromagnetic Formalism

Established in 1870, Maxwell's equations are fundamental laws of physics. They constitute the basic theories of electromagnetism. These equations provide relationships between the variations of the four characteristic vectors of the electromagnetic field: the electric field E (V/m), the magnetic field H (A/m), the electric flux density D (C/m^2), and the magnetic flux density B (T) at any point in space.

Time-dependent variations are expressed by the partial derivative with respect to time, and spatial variations by the differential operators: curl and divergence.

At any point in space, which is not located on a surface separating two media, that is to say, in a linear, homogeneous, and isotopic (LHI) medium, Maxwell's general equations specify that [48]-[51]:

$$\nabla \times \boldsymbol{E}(t,r) = -\frac{\partial \boldsymbol{B}(t,r)}{\partial t} \tag{11}$$

$$\nabla \times \boldsymbol{H}(t,r) = \boldsymbol{J}(t,r) + \varepsilon_0 \frac{\partial \boldsymbol{E}(t,r)}{\partial t} \tag{12}$$

$$\nabla \cdot \boldsymbol{D}(t,r) = \rho(t,r) \tag{13}$$

$$\nabla \cdot \boldsymbol{B}(t,r) = 0 \tag{14}$$

The basic variables of these equations are [49]:

$\boldsymbol{B}$: Magnetic induction (Tesla, T)

$\boldsymbol{H}$: Magnetic field strength (Ampere/ meter^2, Am^{-2})

$\boldsymbol{D}$: Electric flux density (colomb/meter^2, cm^{-2})

$\boldsymbol{E}$: Electric field density (volts/meter, Vm^{-1})

$\boldsymbol{J}$: Electric current density (ampere/ meter^2, Am^{-2})

ρ: Electric charge density (coulomb/meter^3, cm^{-3})

With [50]:

$$\boldsymbol{B} = \mu \boldsymbol{H} \tag{15}$$

$$\boldsymbol{D} = \varepsilon \boldsymbol{E} \tag{16}$$

$$\boldsymbol{J} = \sigma \boldsymbol{E} \tag{17}$$

And [51]:

μ: Magnetic permeability;

ε: Electrical permeability;

σ: Electrical conductivity.

In this form, called local or differential, Maxwell's equations express relationships between spatial variations of some fields and temporal variations of other fields.

Into the void:

$$\boldsymbol{B}(t,r)=\mu_0\boldsymbol{H}(t,r) \tag{18}$$

$$\boldsymbol{D}(t,r)=\varepsilon_0\boldsymbol{E}(t,r) \tag{19}$$

Then Maxwell's equations become:

$$\nabla\times\boldsymbol{H}(t,r)=\varepsilon_0\frac{\partial\boldsymbol{E}(t,r)}{\partial t} \tag{20}$$

$$\nabla\cdot\boldsymbol{H}(t,r)=0 \tag{21}$$

$$\nabla\cdot\boldsymbol{B}(t,r)=0 \tag{22}$$

The differential operator nabla ∇ is used to express the curl operation $\nabla\times$ = rot and the divergence operation $\nabla\cdot$ = div .

Maxwell's equations can also be expressed in "global form" as follows [51] [52]:

$$\oint_c\boldsymbol{E}(t,r)\mathrm{d}\boldsymbol{l}=-\int_s\boldsymbol{n}\frac{\partial\boldsymbol{B}(t,r)}{\partial t}\mathrm{d}A \tag{2 3}$$

$$\oint_c\boldsymbol{H}(t,r)\mathrm{d}\boldsymbol{l}=-\int_s\boldsymbol{n}\left(\frac{\partial\boldsymbol{D}(t,r)}{\partial t}+\boldsymbol{J}(t,r)\right)\mathrm{d}A \tag{24}$$

Using the divergence theorem after integrating Equations (23) and (24), Equations (13) and (14) then become:

$$\oint_c\boldsymbol{n}\boldsymbol{D}(t,r)\mathrm{d}A=\int_v\rho(t,r)\mathrm{d}A \tag{25}$$

$$\int_s\boldsymbol{n}\boldsymbol{B}(t,r)\mathrm{d}A=0 \tag{26}$$

The boundary conditions for fields [52] are:

$$\boldsymbol{n}\times\left[\boldsymbol{E}_1(t,r)-\boldsymbol{E}_2(t,r)\right]=0 \tag{27}$$

$$\boldsymbol{n}\times\left[\boldsymbol{H}_1(t,r)-\boldsymbol{H}_2(t,r)\right]=\boldsymbol{j}_S \tag{28}$$

$$\boldsymbol{n}\times\left[\boldsymbol{D}_1(t,r)-\boldsymbol{D}_2(t,r)\right]=\rho_S \tag{29}$$

$$\boldsymbol{n}\times\left[\boldsymbol{B}_1(t,r)-\boldsymbol{B}_2(t,r)\right]=0 \tag{30}$$

With:

$\boldsymbol{n}$: is the normal to the separation surface, going from midpoint 2 to midpoint 1;

$\boldsymbol{j}_S$: is the surface current density;

ρ_S : is the surface charge density.

Starting from the wave equations below obtained from Maxwell's equations, for the electric and magnetic fields of interest, the wave equations, at a point $\boldsymbol{r}$ and at time t, are given respectively by [47]-[51]:

$$\nabla \times \nabla \times \boldsymbol{E}(\boldsymbol{r},t) + \mu_0 \varepsilon_0 \frac{\partial^2}{\partial t^2} \boldsymbol{E}(\boldsymbol{r},t) = \mu_0 \frac{\partial^2}{\partial t^2} \boldsymbol{J}(\boldsymbol{r},t) \tag{31}$$

$$\nabla \times \nabla \times \boldsymbol{H}(\boldsymbol{r},t) + \mu_0 \varepsilon_0 \frac{\partial^2}{\partial t^2} \boldsymbol{H}(\boldsymbol{r},t) = \mu_0 \nabla \times \boldsymbol{J}(\boldsymbol{r},t) \tag{32}$$

where $\boldsymbol{E}$ is the electric field $\boldsymbol{H}$ is the magnetic field and μ_0 and ε_0 are respectively the magnetic permeability and electric permittivity of air (vacuum). The wave equations are written as follows [51]:

$$\Delta \boldsymbol{E}(\boldsymbol{r},t) - \mu_0 \varepsilon_0 \frac{\partial^2}{\partial t^2} \boldsymbol{E}(\boldsymbol{r},t) = \frac{1}{\varepsilon_0} \nabla \rho(\boldsymbol{r},t) + \mu_0 \frac{\partial}{\partial t} \boldsymbol{J}(\boldsymbol{r},t) \tag{33}$$

$$\nabla \times \nabla \times \boldsymbol{H}(\boldsymbol{r},t) + \mu_0 \varepsilon_0 \frac{\partial^2}{\partial t^2} \boldsymbol{H}(\boldsymbol{r},t) = \nabla \times \boldsymbol{J}(\boldsymbol{r},t) \tag{34}$$

where ε and μ are characteristic of the medium considered and represent, respectively, the permittivity and permeability of the medium. These quantities allow us to define the propagation speed v and the characteristic impedance of the medium η by the following relations:

$$\begin{cases} v = \dfrac{1}{\sqrt{\mu\varepsilon}} \text{ vitesse de propagation en m/s} \\ Z = \sqrt{\dfrac{\mu}{\varepsilon}} \text{ impedance du milieu en } \Omega \end{cases} \tag{34a}$$

3.2. Modeling the Propagation of EM Waves Radiated by GSM Relay Antennas

3.2.1. FDTD Digital Model

However, depending on the type of problem one wishes to study, there are several ways to rewrite Maxwell's equations [52]-[55]. Today, with the increasing power of computing tools, several numerical tools and methods exist for translating the behavior of these equations. In this study, we implement the FDTD method [53] because it can simulate the behavior of an electromagnetic wave in any type of medium (dielectric, vacuum, metal, plasma, etc.), while taking into account the most complex geometric shapes of the objects that may constitute the system [54].

It does not involve any matrix inversion. Its extremely simple theoretical formulation provides highly accurate predictions for a wide range of problems in the electromagnetic domain [52]-[55]. It is characterized by a broad bandwidth; an impulse excitation in the time domain is sufficient to give the response of a system over a wide frequency range via a Fourier transform [55]. In this method, the unknowns are the electric and magnetic $\boldsymbol{B}$ fields $\boldsymbol{E}$.

The principle consists of approaching the spatial and temporal derivatives with finite differences using an explicit scheme: this means that at each time step, it is possible to calculate all the derivatives without having to invert matrices [52]-[55].

The points where E and H are calculated are offset by half a step, in space and

in time. For each half-step of time, the values of the E and H fields are updated alternately. Using a uniform grid in Cartesian coordinates, the following Figure 6: $\Delta x = \Delta y = \Delta z = \Delta$, the indices in the *x, y, z directions* are *i, j, k*; the time step is Δt and therefore, the time is: $n.\Delta t$.

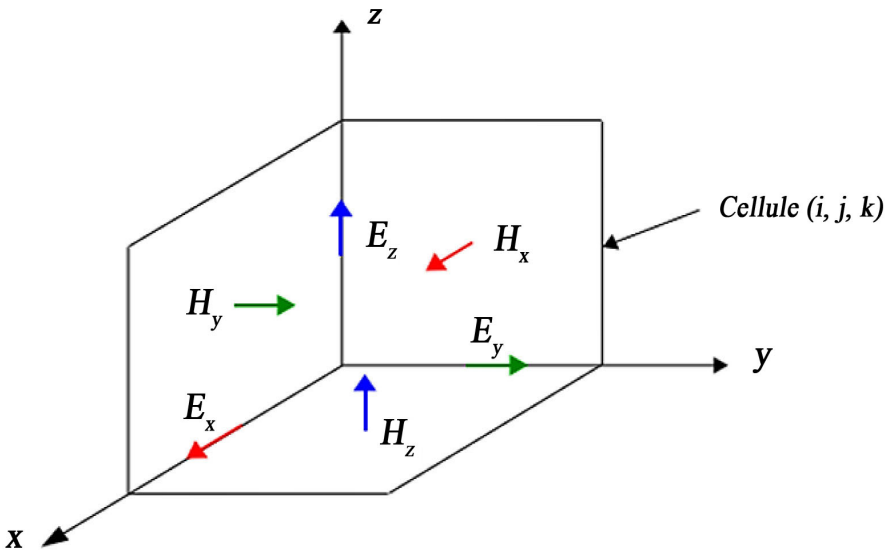

Figure 6. Yee cell.

The centered difference approximation is applied subsequently [52]-[55]:

$$\begin{cases} \nabla \times \boldsymbol{E}^i = -\mu_0 \dfrac{\partial \boldsymbol{H}^i}{\partial t} \\ \nabla \times \boldsymbol{H}^i = \varepsilon_0 \dfrac{\partial \boldsymbol{E}^i}{\partial t} \end{cases} \tag{35}$$

The dielectric parameters ε, μ and σ *are* time-independent, so the two previous equations can be written as follows in the system (*x, y, z*) [52]-[55]:

$$\begin{cases} \dfrac{\partial H_x}{\partial t} = \dfrac{1}{\mu}\left(\dfrac{\partial H_y}{\partial z} - \dfrac{\partial H_z}{\partial y}\right) \\ \dfrac{\partial H_y}{\partial t} = \dfrac{1}{\mu}\left(\dfrac{\partial H_z}{\partial x} - \dfrac{\partial H_x}{\partial z}\right) \\ \dfrac{\partial H_z}{\partial t} = \dfrac{1}{\mu}\left(\dfrac{\partial H_x}{\partial y} - \dfrac{\partial H_y}{\partial x}\right) \\ \dfrac{\partial E_x}{\partial t} = \dfrac{1}{\mu}\left(\dfrac{\partial H_z}{\partial y} - \dfrac{\partial H_y}{\partial z} - \sigma E_x\right) \\ \dfrac{\partial E_y}{\partial t} = \dfrac{1}{\mu}\left(\dfrac{\partial H_x}{\partial z} - \dfrac{\partial H_z}{\partial x} - \sigma E_y\right) \\ \dfrac{\partial E_z}{\partial t} = \dfrac{1}{\mu}\left(\dfrac{\partial H_y}{\partial x} - \dfrac{\partial H_x}{\partial y} - \sigma E_z\right) \end{cases} \tag{36}$$

E_x, E_y, E_z and H_x, H_y, H_z are the components of $\boldsymbol{E}$ and $\boldsymbol{H}$ respectively. Subsequently, we calculate the three components of E and H:

$$\begin{cases} \dfrac{\partial E_y(x,y,z,t)}{\partial x} = \dfrac{E_y^n(i+1/2,j,k) - E_y^n(i-1/2,j,k)}{\Delta t} \\ \dfrac{\partial E_y(x,y,z,t)}{\partial t} = \dfrac{E_y^{n+1/2}(i,j,k) - E_y^{n-1/2}(i,j,k)}{\Delta t} \\ E_x^{n+1}(i+1/2,j,k) = A_{i+1/2,j,k} E_x^n(i+1/2,j,k) \\ \quad + B_{i+1/2,j,k}\left[H_z^{n+1/2}(i+1/2,j+1/2,k) - H_z^{n+1/2}(i+1/2,j-1/2,k)\right] \\ \quad + B_{i+1/2,j,k}\left[H_y^{n+1/2}(i+1/2,j,k-1/2) - H_y^{n+1/2}(i+1/2,j,k+1/2)\right] \\ H_x^{n+1}(i,j+1/2,k+1/2) = H_y^{n-1/2}(i+1/2,j,k+1/2) \\ \quad + \dfrac{\Delta t}{\mu\delta}\left[E_y^n(i,j+1/2,k+1) - E_y^n(i,j+1/2,k)\right] \\ \quad + \dfrac{\Delta t}{\mu\delta}\left[E_z^n(i+1/2,j,k-1/2) - E_z^n(i,j+1,k+1/2)\right] \end{cases} \tag{37}$$

Or:

$$\begin{cases} A_{i,j,k} = 1 - \dfrac{\sigma(i,j,k)}{\varepsilon(i,j,k)} \\ B_{i,j,k} = \dfrac{\Delta t}{\varepsilon(i,j,k)\delta} \end{cases} \tag{38}$$

3.2.2. Hertzian Dipole Model

The use of dipole theory not only simplifies the general expressions of electromagnetic fields radiated by GSM relay antennas, but also allows modeling of EM radiation emitted by a radiating structure from knowledge of the currents involved [56]-[59].

The EM fields radiated by a GSM relay antenna can be estimated by considering an infinitesimal portion of length *dl* of the line carrying a constant current as a radio dipole. The EM fields created by this antenna are then considered to correspond to the superposition of the fields produced by all the dipoles constituting the wire structure [56]. It is assumed that the current distribution is variable along the antenna, but that the current is constant for each elementary dipole (see **Figure 7**) [57]. The accuracy of the method is then governed by the number of dipoles required to adequately represent this current distribution [56]-[59]. The greater the number of dipoles, the better the accuracy [56]-[59].

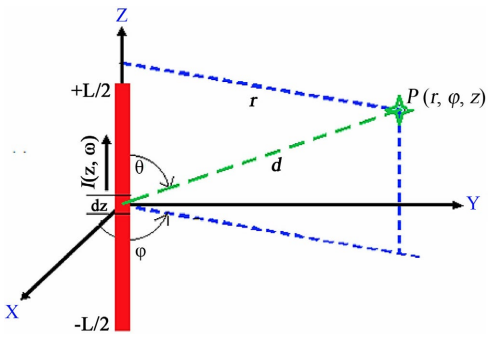

Figure 7. Geometry of a GSM relay antenna [56]-[59].

Consider a wire antenna of length, centered at the origin of the coordinate system and parallel to the axis (z). The antenna in **Figure 7** carries a sinusoidal current (I), $\omega = 2\pi f$ where f represents the frequency [56]-[59].

This antenna is considered as a superposition of N elementary dipoles of identical lengths dz such that: $L = N \cdot dz$. The observation point P is located at any position in space [58]. The vector potential created by this structure at a given point is simply the contribution of the elementary vector potentials constituting the wire antenna, *i.e.* [59]:

$$\begin{cases} \delta \boldsymbol{A} = \dfrac{\mu I}{4\pi} G_0\left(\gamma_s, d\right) dz \cdot \boldsymbol{e}_z = \delta A_z \cdot \boldsymbol{e}_z \\ \boldsymbol{A} = \displaystyle\sum_{i=1}^{N} \delta \boldsymbol{A}_i \\ \boldsymbol{A} = \dfrac{\mu N}{4\pi L} \displaystyle\sum_{i=1}^{N} I\left(z_i, \omega\right) G\left(\gamma_s, d_i\right) \boldsymbol{e}_z \end{cases} \tag{39}$$

Similarly, the expressions for electromagnetic fields obtained for an infinitesimal dipole can be generalized to the case of an antenna satisfying the thin-wire assumptions [56]-[59]. These assumptions assume that the current does not undergo azimuthal variation and is uniformly distributed over the surface of the cable. This is valid if the radius is small compared to the wavelength and the distance from the interface. Thus, the electromagnetic fields radiated by this antenna are simply deduced by summing the elementary fields, hence [56]-[59]:

$$\begin{cases} \boldsymbol{E} = \displaystyle\sum_{i=1}^{N} \delta \boldsymbol{E}_i \\ \boldsymbol{H} = \displaystyle\sum_{i=1}^{N} \delta \boldsymbol{H}_i \end{cases} \tag{40}$$

The expansion of the expressions for the elementary fields of Equation (30), obtained in **Figure 7**, the non-zero components of the electromagnetic fields in a cylindrical coordinate system $\left(\boldsymbol{e}_r, \boldsymbol{e}_\varphi, \boldsymbol{e}_z\right)$, are written for a wire antenna:

$$\begin{cases} H_\varphi = \dfrac{-L}{4\pi N} \displaystyle\sum_{i=1}^{N} I\left(z_i, \omega\right) \sin\left(\theta_i\right) \dfrac{\partial G\left(\gamma_s, d_i\right)}{\partial d_i} \\ E_r = \dfrac{\eta L}{8\pi \gamma N} \displaystyle\sum_{i=1}^{N} I\left(z_i, \omega\right) \sin\left(2\theta_i\right) \left(\dfrac{\partial^2 G\left(\gamma_s, d_i\right)}{\partial d_i^2} - \dfrac{1}{d_i} \dfrac{\partial G\left(\gamma_s, d_i\right)}{\partial d_i} \right) \\ E_z = \dfrac{\eta L}{4\pi \gamma N} \displaystyle\sum_{i=1}^{N} I\left(z_i, \omega\right) \left(\cos^2\left(\theta_i\right) \dfrac{\partial^2 G\left(\gamma_s, d_i\right)}{\partial d_i^2} + \dfrac{\sin^2\left(\theta_i\right)}{d_i} \dfrac{\partial G\left(\gamma_s, d_i\right)}{\partial d_i} - \gamma^2 G\left(\gamma_s, d_i\right) \right) \end{cases} \tag{41}$$

3.2.3. Empirical Evaluation Methods

The evaluation of electromagnetic fields (EMF) from GSM antennas using empirical models relies on propagation formulas (free space, Okumura-Hata) that take into account the EIRP (Equivalent Isotropically Radiated Power) [60], antenna gain, distance, and environment to estimate the power density and electric field (V/m), and then deduce the magnetic field. These models predict far-field signal attenuation [61]. These methods are generally used for pre-installation estimations or theoreti-

cal checks, with actual on-site measurements required for full accuracy [62].

Empirical models for evaluating the electromagnetic fields (EMF) of GSM antennas, such as propagation models (Hata, COST-231), estimate exposure based on real measurements rather than complex physical simulations. They use simplified formulas incorporating power, antenna gain, frequency, and distance [60]-[62].

Advantages [60]-[62]:

- Speed: Fast calculations with low computing resource consumption.
- Simplicity: Usable for general coverage assessments without complex 3D modeling.
- Adaptability: Suitable for GSM frequencies (900/1800 MHz) in urban or rural environments.

Weaknesses [63]-[65]:

- Limited accuracy: Less accurate than deterministic models (ray tracing) in complex environments.
- Data dependency: Requires precise technical information (antenna diagrams, tilt) which is sometimes difficult to obtain.
- Specific cases: Less effective at predicting the far field or the impact of unique obstacles.
- These models are useful for an initial estimation of overall exposure, but often require validation through field measurements.

The power density vector, Poynting vector S, of an electromagnetic field is given by the cross product of the electric component E and the magnetic component H of the field [63]-[65]:

$$S = E \times H \tag{42}$$

Ideal conditions [63]-[65], that is, when it is important that the ground or other obstacles have no influence, this equation can be simplified because the electric field, the magnetic field, and the direction of propagation are perpendicular to each other. Furthermore, the ratio of the amplitudes of the electric field, E, and the magnetic field, H, is a constant Z_0, called the characteristic impedance of free space, equal to approximately 377 Ω (or 120π Ω).

Thus, in the far-field region, the free-space power density, S, is given by the following non-vector equation [63]-[65]:

$$S = \frac{E^2}{Z} = \frac{H^2}{Z_0} \tag{43}$$

In general, the characteristic impedance of a medium is given by the formula: $Z = \sqrt{\frac{\mu}{\varepsilon}}$ where μ is the magnetic permeability (μ = 1.2566 × 10^6 F/m in free space) and ε is the permittivity (= 8.85418 × 10^{12} H/m in free space) [63]-[65].

The power density regardless of distance and direction can be calculated in the far-field region using the following equation:

$$S = P\frac{G_i}{4\pi r^2} \tag{44}$$

where [63]-[65]:

S: power density (W/m^2) in a given direction

P: power (W) supplied to the radiation source, assuming a lossless system

G_i: gain factor of the radiation source in the direction considered, relative to an isotropic radiating element

r: distance (m) from the radiation source.

$P{\cdot}G_i$ product In Equation (44), EIRP is called the EIRP and represents the power that a fictitious isotropic radiating element would have to emit to produce the same field strength at the receiving point. The antenna pattern must be taken into account for power densities in other directions [66]-[68].

To use Equation (44) with an antenna whose gain G_a is related to a reference antenna of isotropic gain G_r, for example a half-wave dipole or a short unipolar antenna, the gain factor G_i must be replaced by the product $G_r{\cdot}G_a$ as in Equation (44). The relevant factor G_r is given in [60]; it is 1.64 for half-wave dipole applications (television, broadcasting on metric waves and sometimes on decametric waves) and 3.0 for short unipolar antennas (broadcasting on kilometric, hectometric, and sometimes decametric waves) [66]-[69]:

$$S = P\frac{G_r G_a}{4\pi r^2} \tag{45}$$

Thus, when the antenna gain G_d ($G_a = G_d$) is referred to that of a half-wave dipole [63]-[65]:

$$S = 1.64 \cdot P\frac{G_d}{4\pi r^2} \tag{46}$$

where: G_d: antenna gain relative to a half-wave dipole.

Similarly, when the antenna gain $G_a = G_m$ is related to that of a short unipolar antenna [63]-[65]:

$$S = 3.0 \cdot P\frac{G_m}{4\pi r^2} \tag{47}$$

where: G_m: antenna gain relative to a short unipolar antenna.

Equations (42) to (46) assume that the conditions are those specific to the far-field region where the field is in the form of a plane wave; they do not concern calculations for the near-field region. If Equation (42) is inserted into Equation (44) to eliminate S and a factor C is introduced to account for the direction characteristic of the radiation source, Equation (47) is obtained, which allows the electric field of a radiation source to be calculated in the far-field region [63]-[65]:

$$E = \sqrt{\frac{Z_0}{4\pi}}\frac{\sqrt{P \cdot G_i}}{r}C = \frac{\sqrt{30P \cdot G_i}}{r}C \tag{48}$$

Or:

E: electric field (V/m);

Z_0 = 377 Ω, characteristic impedance of free space;

P: power supplied to the radiation source (W), assuming a lossless system;

C: factor ($0 \le C \le 1$) which takes into account the direction characteristic of the

radiation source (in the principal direction of the radiation, $C = 1$).

If the antenna gain is referred to that of a half-wave dipole or a short unipolar antenna and not to that of an isotropic radiating element, it is appropriate to use instead of G_i the factors G_d and G_m respectively in Equations (49) and (50) [63]-[65].

$$E = \sqrt{\frac{Z_0}{4\pi}} \frac{\sqrt{1.64P \cdot G_d}}{r} C = \frac{\sqrt{49.2P \cdot G_d}}{r} C \tag{49}$$

$$E = \sqrt{\frac{Z_0}{4\pi}} \frac{\sqrt{3P \cdot G_m}}{r} C = \frac{\sqrt{90P \cdot G_m}}{r} C \tag{50}$$

To calculate the magnetic field, in the far-field region, of a radiation source, Equation (51) [63]-[65] is used:

$$H = \frac{E}{Z_0} \tag{51}$$

Or:

E: electric field (V/m);

H: magnetic field (A/m);

Z_0 = 377 Ω (120π), characteristic impedance of free space.

4. Equipment and Protocols for Measuring Electromagnetic Fields Radiated by GSM Relay Antennas

Based on existing work in the literature [60]-[64], to measure the electromagnetic fields (EMF) of GSM base stations, researchers use professional EMF detectors such as probes, spectrum analyzers, calibrated, following strict protocols such as those of the ANFR (National Frequency Agency), which involve measurements at various points (indoors, outdoors), taking into account the frequencies (GSM, 3G, 4G, 5G) and the operators [61], to compare the measured values with the regulatory limits (expressed in V/m) established to protect the public, with extrapolation calculations for maximum power scenarios [62]-[64]. The measurement protocol in operational terms takes into account the type of sensor, isotropy, averaging time, sampling duration, height above ground, number of repetitions per point.

4.1. Measuring Equipment

The equipment used for geolocating measurement points and quantifying electromagnetic fields, taken from existing literature [65]-[68], is:

- Location systems: GPS to geolocate measurement points [65]. For confirmation of the choice of measurement areas, the HF DIGIMETER Endotronic D8826 can be used, which is an electromagnetic radiation meter focused on measuring noise voltage.
- Electric (E) and magnetic (B) field probes: Specific to telecommunications frequencies (from a few MHz to several GHz), often with triaxial probes to cover all directions [66].

- Spectrum analyzers: To identify the different sources (operators, technologies) and their respective frequencies [67].
- Software: For data acquisition, processing and results mapping [67].

4.2. Measurement Protocols (According to the ANFR/COMSIS Framework)

According to the ANFR/COMSIS framework [67], a good RF/GSM electromagnetic measurement protocol should include the following aspects:

- Definition of zones: Residential premises, public places (parks, shops), places accessible to the public.
- Antenna location: Use of Cartoradio (ANFR website) to identify sources.
- On-site measurements [65]-[67]:
  - Measurement points: At height (1.5 m) and in the corners of rooms for the interior; at various locations outside.
  - Scenarios: Measurements in real-world conditions (low/high number of users) and theoretical extrapolation (all antennas at maximum power).
  - Frequencies: Taking into account the different bands (GSM, 3G, 4G, 5G).
- Calculation of limit values: The results are compared to the limit values set by decree (e.g., 5 V/m at 900 MHz for the public).
- Analysis of results [65]-[67]:
  - Comparison with thresholds: Verification that exposure remains below regulatory limit values.
  - Mapping: Creation of exposure level maps by area.
  - Reports: Preparation of detailed reports by accredited bodies (such as Apave or others) to assess compliance with standards.

4.3. Metric Method and Evaluation Criteria for Simulation Methods in Relation to Measurements

The metric method describes Data Analysis (or Statistical Analysis), which uses systematic techniques (statistical and logical) to describe, structure, condense, visualize (images, tables, graphs) and evaluate biases in data, in order to draw meaningful conclusions, often combining descriptive and inferential statistics to understand phenomena and make predictions [69].

We reiterate that one of the objectives of this article is to contribute to the definition of an exposure indicator by jointly exploiting aspects related to measurements and simulations. One of the means used to achieve this objective is to focus on indicators for evaluating errors between measurements and simulations [69]. Given the number of exposure situations that may need to be studied, finding a relevant comparison indicator suitable for all exposure cases is not a trivial matter. The question of the criterion for evaluating prediction error has therefore become a crucial problem in the search for an exposure indicator to enable [69]:

- to conduct a mutual validation of the methods and protocols used;

- analyze the uncertainties related to the calculation methods;
- to best characterize all exposure configurations;
- develop lower cost monitoring systems.

In this section, we will present a state-of-the-art review of reliability indicators for calculation methods commonly used in radio wave simulation. From this, we will identify a relevant criterion for evaluating prediction errors to meet all our requirements.

The criteria for comparing prediction methods with measurements generally used in radio wave simulation can be classified according to 3 types of criteria:

- The "error" type criterion;
- The "link" type criterion;
- The criterion of type "characteristics of the data distribution".

Equation (52) presents the equations modeling the criteria described above. For further details, we recommend that researchers consult the bibliographic references [69]. These indicators allow for the search for a linear relationship between measurements and simulations. However, depending on the variability of the data distribution, the results may lead to erroneous conclusions. They are better suited to normally distributed data without exceptional values.

Therefore, in the context of evaluating methods for simulating exposure, due to the high variability of exposure, their use is not appropriate, especially in exposure cases.

This is because a very high value and a very low value can be found at two relatively close points, as everything depends on the point's position relative to the antenna and the medium through which the wave propagates.

$$\begin{cases} MeanError = \dfrac{1}{N}\sum_{i}^{N}\left(X_i - Y_i\right) \\ \sigma_x = \dfrac{1}{N}\sum_{i}^{N}\left(X_i - \bar{X}\right)^2 \\ \sigma_y = \dfrac{1}{N}\sum_{i}^{N}\left(Y_i - \bar{Y}\right)^2 \\ RMSE = \sqrt{\dfrac{\sum_{i}^{N}\left(X_i - Y_i\right)^2}{N}} \\ P = \dfrac{Cov\left(X,Y\right)}{\sigma_x \sigma_y} \\ Cov\left(X,Y\right) = \dfrac{1}{N}\sum_{i}^{N}\left(X_i - \bar{X}\right)\left(Y_i - \bar{Y}\right) \end{cases} \tag{52}$$

5. Results of Simulations and Measurements

5.1. Declaration of Simulation Parameters and Measurement Tools for EM Waves

5.1.1. GSM Sites

See Table 1 below:

Table 1. GSM site characteristics.

Location	S-4.311744 and E 15.293357
Safety zone template type	Iron bar
Size of the security zone	10 m × 12 m
Fence height	2 meters
Floor covering	Concrete/gravel
Technology to be implemented	4G
Typology from the perspective of bays	ground -level bays
Typology from the perspective of antennas	Antennas on pylons in open terrain
Pylon height	50 meters
Typology from an occupational point of view	Potential shared site
Nature of the site in relation to the network	BTS
Number of sectors	3
Number of transceivers per sector	2
Antenna power	125mW
Gain	21 dB
Location	S-4.311744 and E 15.293357
EIRP per sector or power conducted per carrier/TRX	20 W per carrier, 43 dBm
Transmission losses	5.3 dB
Antenna model/pattern	GSM 1800 MHz (DCS 1800)
Azimuth	0˚ 120˚ 240˚

5.1.2. Field Measurements

Beyond the responses, most of which were subjective, obtained in the user survey, a more objective quantification of the exposure level seemed necessary. We therefore conducted field measurements in targeted areas, without which comparison to relevant standards would be impossible.

5.1.3. Selection of Measurement Zones

The measurements were carried out in the Gombe district, identified not only as the city center but also as the area most exposed to non-ionizing radiation (NIR) due to the presence of numerous telecommunications antennas. This location is of particular interest because it encompasses a high concentration of socio-economic activity. Consequently, the number of potential subscribers exceeds that of other districts and even the entire Lukunga district. Numerous GSM sites are in-

stalled there, justifying the importance of this study area.

The choice of measurement zones is based on two fundamental criteria: a geometric criterion and a demographic or urban planning criterion. On the one hand, the cellular subdivision inherent to GSM technology allows for the concentration of non-invasive radiofrequency (NIR) in certain specific areas of the municipality. On the other hand, areas with high population density, as well as those exhibiting high sensitivity characteristics, such as hospitals, were also selected due to their increased vulnerability to the effects of NIR.

To delineate these zones, a satellite image of the Gombe district was obtained using Google Earth (version 5.2.1.1588). Two orthogonal axes were drawn, one parallel to Tshatshi Avenue, and two diagonals connecting the four corners of the Golf neighborhood. These axes defined the areas of interest for the measurements.

On each axis and diagonal, measurement points were selected, with between two and four points per axis, excluding the central point (zone 9). Thus, zones 1, 5, 10 and 12 are located on diagonal A; zones 3, 7, 11 and 13 on diagonal B; zones 2, 6 and 14 on the minor axis; and zones 4 and 8 on the major axis.

The geodetic coordinates of the measurement points were extracted directly from Google Earth. A field validation campaign was then carried out using a Garmin eTrex H GPS receiver, allowing for confirmation or adjustment of the coordinates, particularly based on the accessibility of the selected sites. **Figure 8** shows the cadastral map detailing the measurement areas.

5.2. Materials Used for the Different Measurements

Radiation measurements require substantial equipment. In addition to the GPS mentioned earlier for confirming the choice of measurement areas, we used the *HF DIGIMETER Endotronic D8826.* This is an electromagnetic radiation meter focused on measuring noise voltage.

The technical specifications of this equipment are presented below:

- Receiver principle: Wideband linear receiver measuring the sum of peak values of resonant amplitude modulations with 3D sound performance.
- Frequency range, measured electromagnetic noise voltage and linearity: 5 KHz - 8 GHz distributed across 3 inputs:
  - Middle BNC input: 5 kHz to 8 GHz (linear 4 GHz) if their intensity is greater than 10 mV;
  - Left BNC input: Same frequency range with a voltage greater than 30 mV;
  - On the right BNC input: very low noise (minimum 40 μV) can still be measured from 10 MHz (linear), and from 3 MHz (non-linear).
- RF signal sensitivity: ± 3 μV, linear for electromagnetic fields;
- Acoustic output with 50 amplifier;
- Antennas: the device is equipped with 5 antennas including a 15 × 1 mm, a 90 × 20 mm, a 45 × 1 mm, a 980 × 10 mm and the AS2002 antenna;

- Battery life: 9 V, 12 mA alkaline battery with approximately 2 hours of performance;
- Power consumption: between 40 and 80 mA, depending on the sound level;
- Weight: ± 200 g;
- Dimensions: 145 × 76 × 30 mm (L × W × H);
- Uncertainty;
- Calibration: The device was supplied to us already calibrated. A conversion chart between the displayed values (VA) for the three inputs and the corresponding electromagnetic noise voltage values (in volts) was included in the user manual. Since no standard is expressed in terms of noise voltage, we sought the assistance of overseas experts to obtain conversion curves between the displayed values and the power density and electric field values obtained by comparison with other field strength meters and spectrum analyzers.

5.3. Sample Characteristics for Measurements and Simulations

This study considers 50 measurement points, comprising 29 outdoor and 21 indoor points, taken from 30 selected sites. At each point identified by its geographic coordinates, we delimited an area of 8 m^2; the GPS used for location had a resolution of ± 4 m. Once the perimeter was defined, we first traversed the corresponding area, device in hand, in a vertical position at a distance of 1 to 2 m from our support (ground or concrete, depending on the location), guided by sound, in search of the point with the highest level of electromagnetic noise. In certain accessible areas, we took several measurements, both indoors and outdoors, but sometimes also at different heights, particularly on buildings.

We then measured the highest value displayed on the screen using the 45 × 1 mm antenna (vertically polarized), first placing it at the right input and then at the center input if the value exceeded the limit measured at the first input. Finally, we used calibration curves to determine the electric field strength and power density values corresponding to each displayed value.

Electromagnetic noise levels, and therefore electric field and power density levels, were measured in all selected areas between July 6th and 14th, 2022, from 9:00 AM to 5:00 PM. Due to the lack of meteorological equipment, we relied on the websites of TV5 and MSN, whose weekly weather forecasts (parameters relevant to this study) for the period in question were described as follows:

- Temperature: 21˚C - 33˚C;
- Relative humidity: 70% - 80% from 9 a.m. to 5 p.m.;
- Sunrise: 06:06;
- Sunset: 17:59.

5.4. Simulation Results

See Figures 8-16 below:

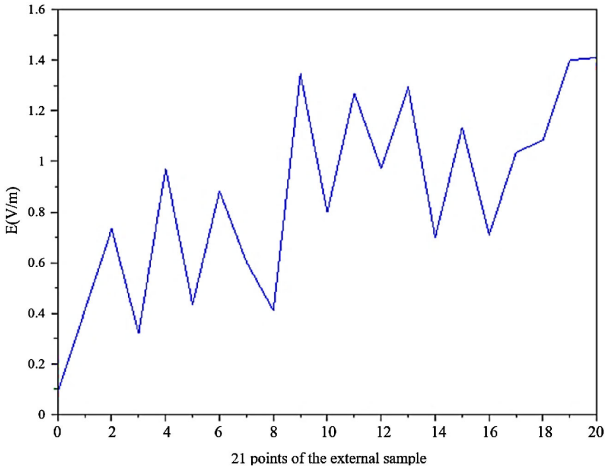

Figure 8. 2D simulation results of the spatial distribution of the electric field on 21 points of the external sample.

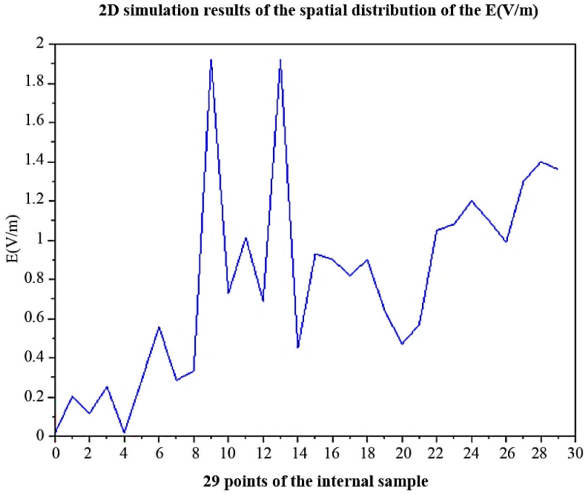

Figure 9. 2D simulation results of the spatial distribution of the electric field on 29 points of the internal sample.

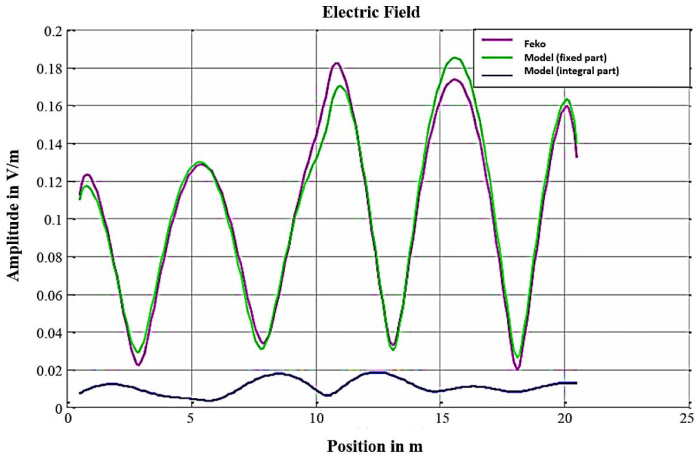

Figure 10. Estimated 2D electric field magnitude as a function of simulation positions [Achraf Liakouti, 2018] [67].

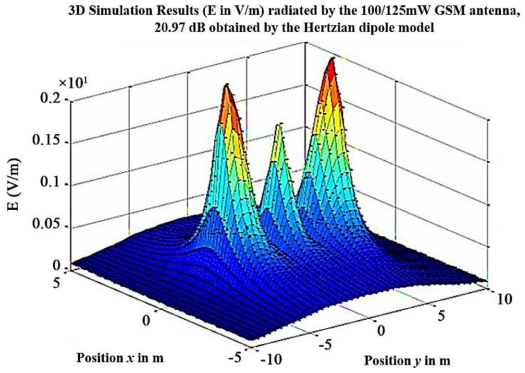

Figure 11. 3D simulation result of the electric field using Hertzian dipole theory.

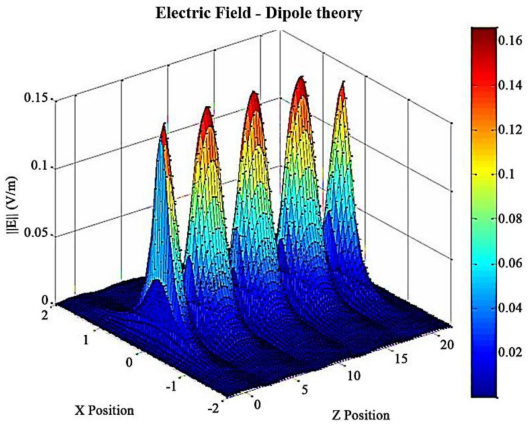

Figure 12. 3D electric field magnitude estimated as a function of measurement position using dipole theory [Achraf Liakouti, 2018] [67].

5.5. Measurement Results

Considering the characteristics of the GSM relay antennas used, those of the measuring instruments used and the climatic conditions of the sample in the chosen geographical area, we obtained the results presented in **Figures 13-23**, **Tables 1-3** below:

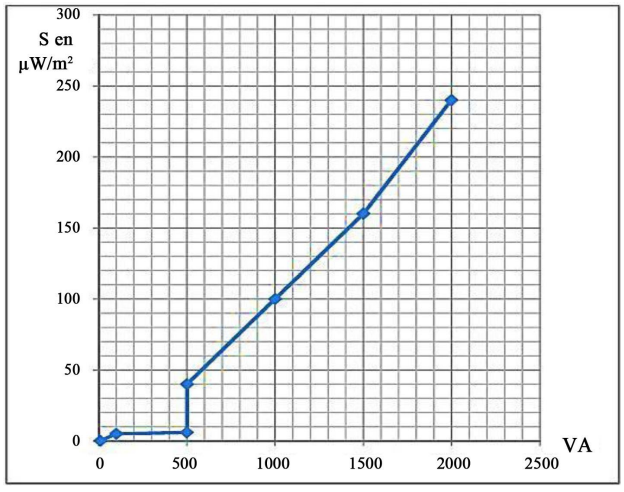

Figure 13. Calibration curve of the right-hand input.

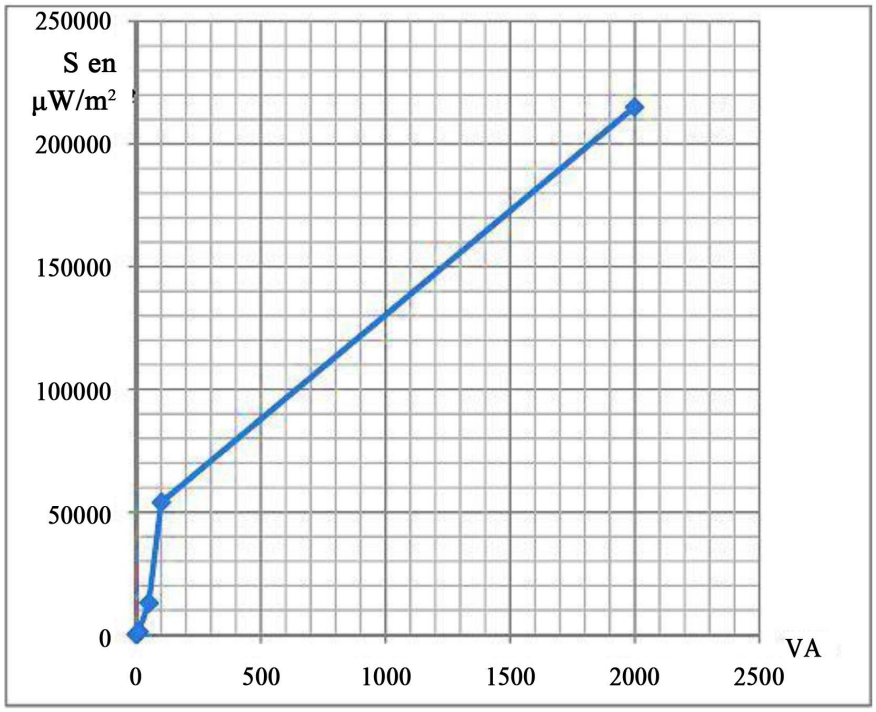

Figure 14. Calibration curve of the center input.

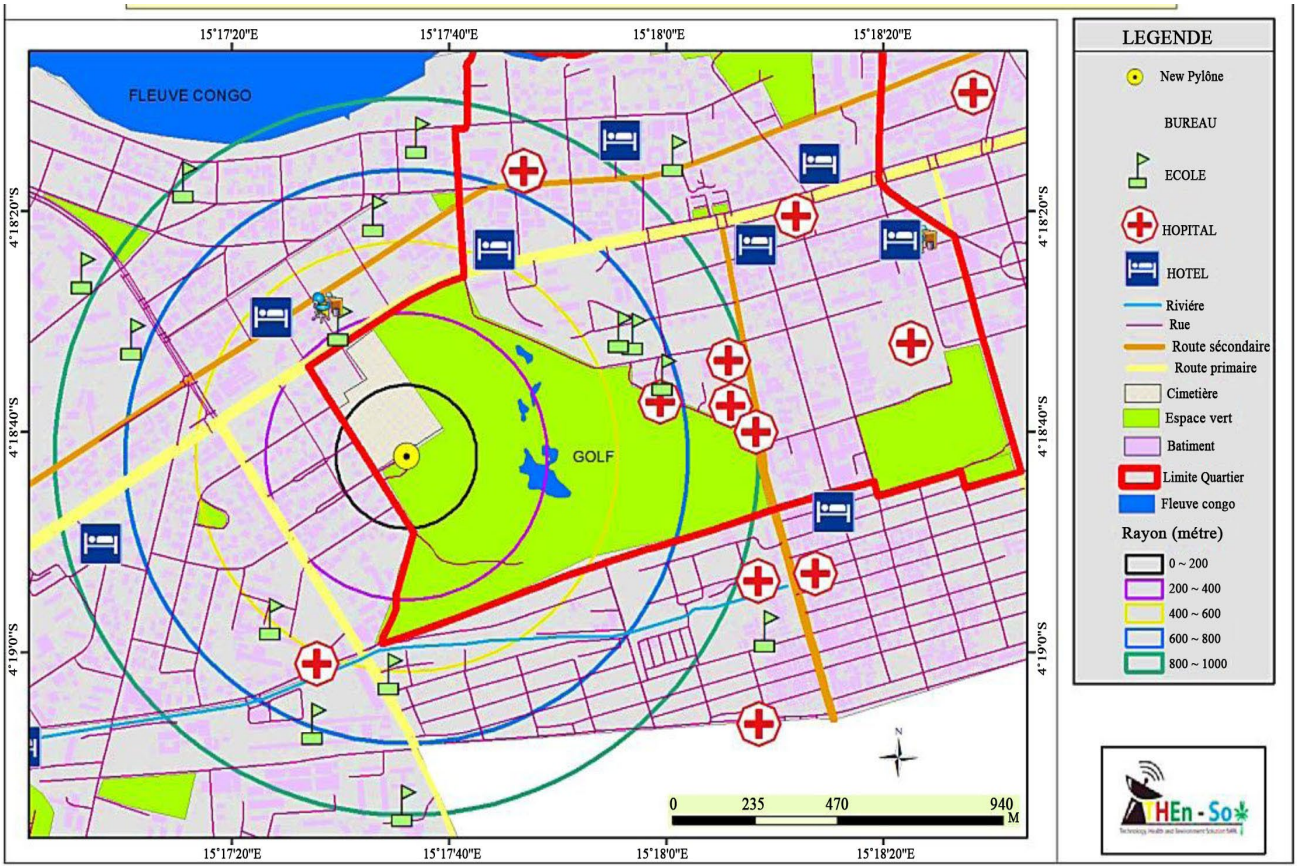

Figure 15. Modeled mapping for assessing the distance between the site and sensitive areas of use.

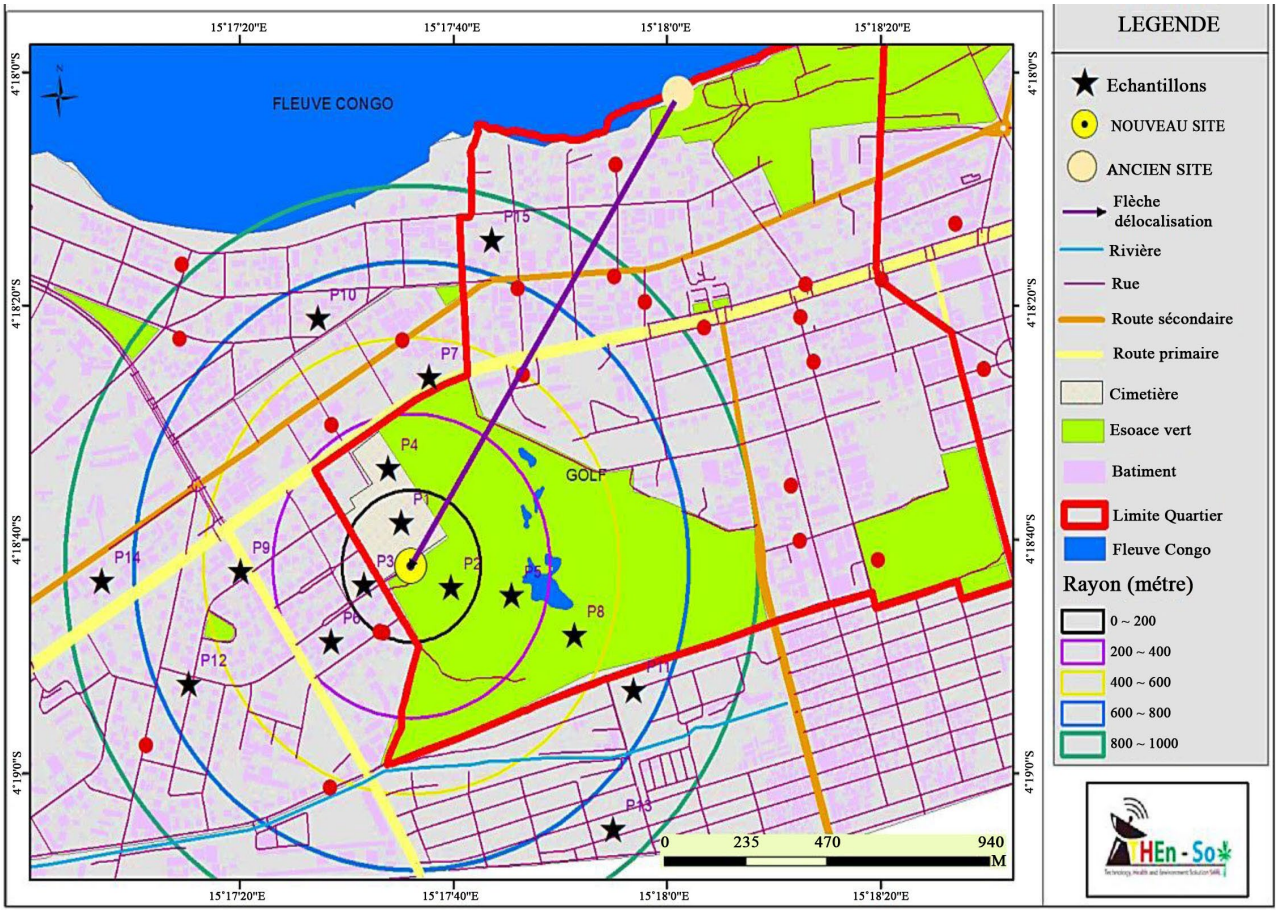

Figure 16. Modeled map of the distribution of measurement points.

Table 2. Statistics of the 50 power density and electric field measurements corresponding.

Statistics	Internal measurements		External measurements		Set of measures	
	E (V/m)	S (W/m²)	E (V/m)	S (W/m²)	E (V/m)	S (W/m²)
Average	0.306925671	0.00445873	0.560242035	0.001106782	0.43358388	0.002829
Minimum	0.13467698	4.8111107	0.441	2.14669E-05	0.51714495	3.47891
Maximum	1.462893613	0.004927	1.382973337	0.00507325	1.372933475	0.00507325
Standard deviation	0.66498790	0.001017997	0.321536724	0.001264807	0.4933117	0.00112232

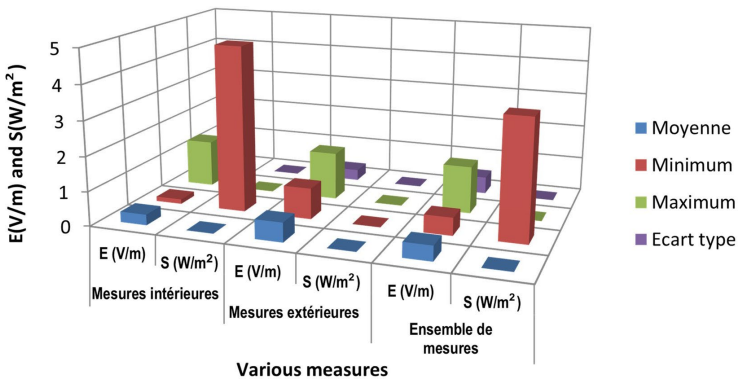

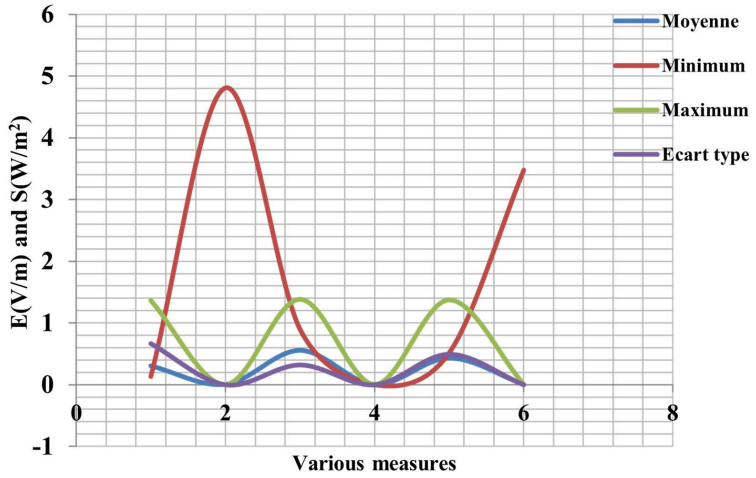

Figure 17. Statistics of the 50 measurements of power density and corresponding electric field.

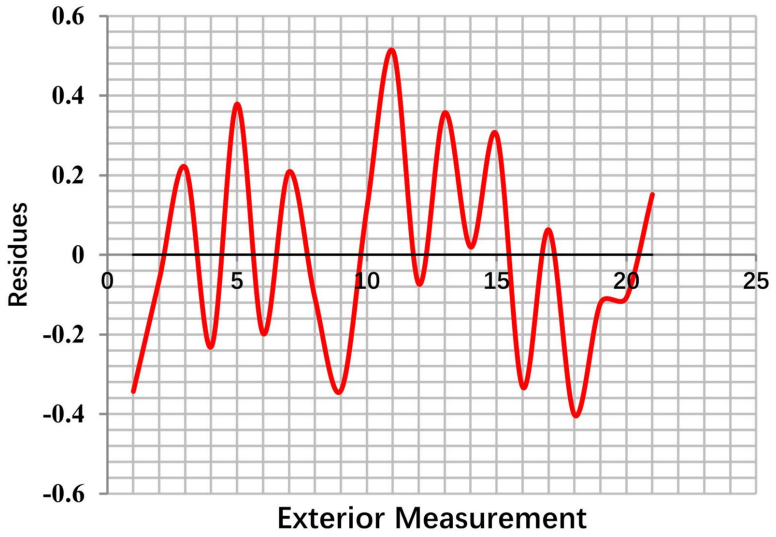

Figure 18. 2D electric field residual graph (external measurement).

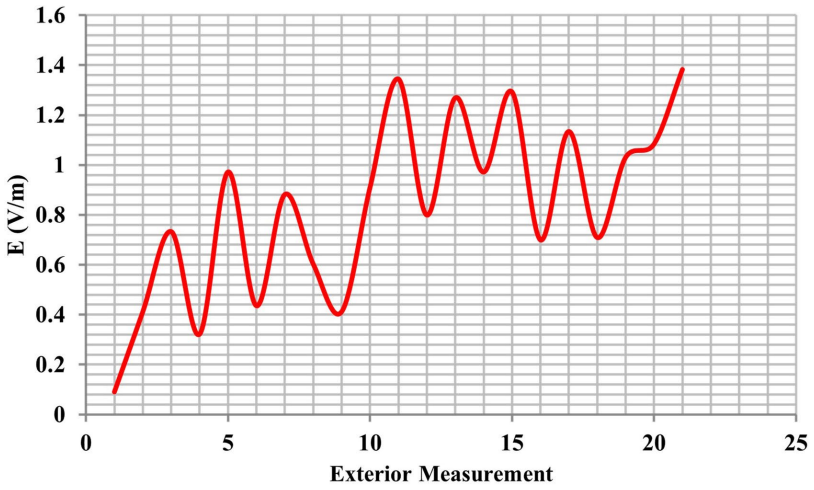

Figure 19. 2D spatial distribution of the electric field (external measurement).

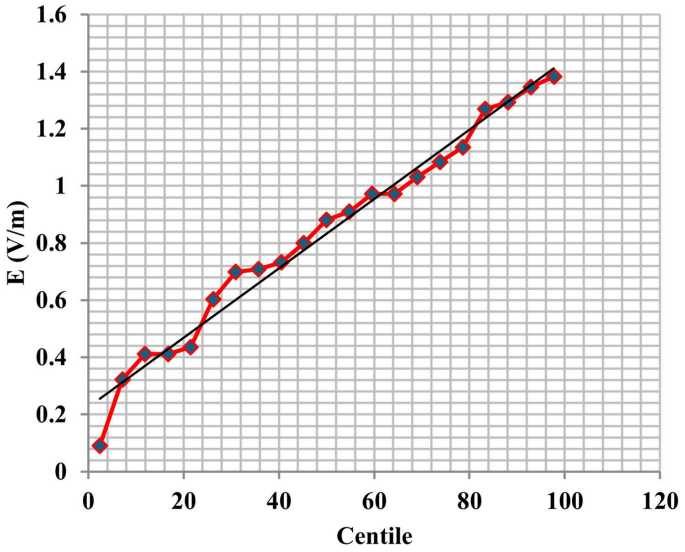

Figure 20. 2D electric field probability distribution (external measurement).

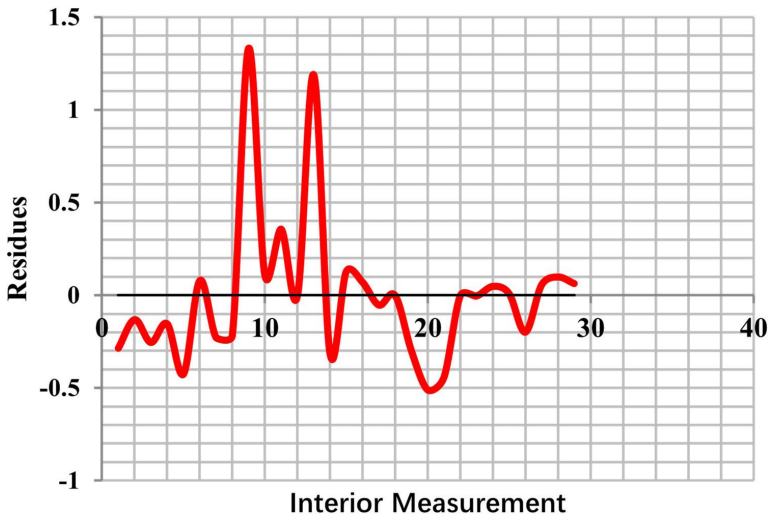

Figure 21. 2D residual graph of the electric field (Indoor Measurement).

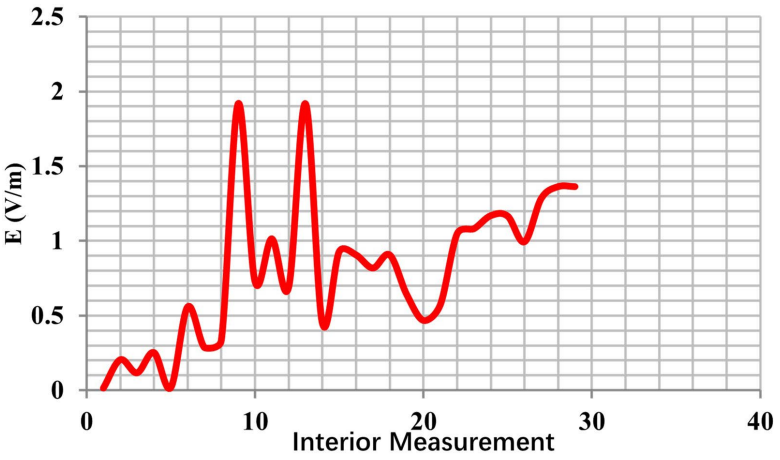

Figure 22. 2D spatial distribution of the electric field (internal measurement).

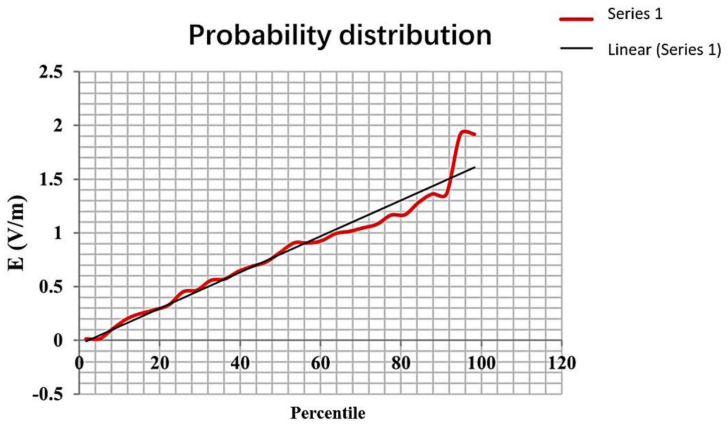

Figure 23. 2D electric field probability distribution: (internal measurement).

Table 3. Joint comparison of 2D simulation and external measurement E (V/m).

No.	Results	Maximum value E (V/m)	Minimum value E (V/m)
01	2D Simulation	1.4	0.1
02	External measurement	1.382973337	0.089961292
03	Gap	0.007	0.01
04	Difference in %	0.7%	1%

Table 4. Joint comparison of 2D simulation and interior measurement E (V/m).

No.	Results	Maximum value E (V/m)	Minimum value E (V/m)
01	2D Simulation	1.92	0.014
02	Interior measurement	1.91	0.013467698
03	Gap	0.01	0.001
04	Difference in %	1%	0.1%

6. Discussions

The massive deployment of GSM mobile phone networks has led to a significant increase in the number of relay antennas, raising concerns about the exposure of populations to electromagnetic fields.

The objective of this article was to model and evaluate the electromagnetic radiation levels emitted by GSM base station antennas in a given geographical area, implementing a joint modeling/measurement analysis. To achieve this, a methodological approach based on field data collection, measurement tools, mathematical modeling of the electromagnetic field using Hertzian dipole theory, and the Okumura-Hata empirical model were implemented to analyze the measured/simulated exposure levels presented below:

Figure 8 shows the 2D simulation result of the spatial distribution of the electric field radiated by GSM antennas at 21 points of the outdoor sample. This electric

field distribution exhibits a sawtooth pattern, with minimum and maximum values of 0.1 V/m and 1.4 V/m, respectively. Figure 9 shows the 2D simulation result of the spatial distribution of the electric field at 29 points of the indoor sample. As can be seen, the electric field profile also exhibits a sawtooth pattern, with minimum and maximum values of 0.014 V/m and 1.92 V/m, respectively. These results corroborate the work presented in the literature by [Achraf] Liakouti, 2018] [67], see Figure 10.

Figure 11 visualizes the 3D simulation result of the electric field profile radiated by GSM antennas based on Hertzian dipole theory. A perfect agreement can be observed between the results from our model based on dipole theory and those obtained by the Feko software in the work proposed by [Achraf] Liakouti, 2018] [67], see Figure 12.

Figures 13-14 show, respectively, the calibration curves for the right input and the center input of the electric field and power density measurement instrument for the GSM antennas under study. The instrument was supplied pre-calibrated. A correlation chart between the displayed values (VA) for the three inputs and the corresponding electromagnetic noise voltage values (in volts) was included in the user manual. Since no standard is expressed in terms of noise voltage, we sought the assistance of experts abroad to obtain correlation curves between the displayed values and the power density and electric field values obtained by comparison with other field strength meters and spectrum analyzers.

Figures 15-16 show the modeled maps for assessing the distance between the site and sensitive areas of use. as well as the distribution of measurement points. It allows for the sampling of measurement points based on the targeted method (LUS) and random sampling (other complementary points). These maps delineate the study areas.

Table 1 and Figure 17 present the statistics of the 50 power density and electric field measurements corresponding. These results showed that the average power density level across all 50 measurements taken was 0.0008292 W/m^2 and the average electric field level was 0.453849162 V/m. This power density value represents 0.041%, 3.455%, and 82.920% of the limit values reported according to the ICNIRP standard, the Brussels-Capital Region standard, and the Salzburg standard, respectively. Regardless of the standard considered among the three, the average level remained below the permissible limit value.

However, these values showed significant differences between them.

Indeed, although no measurement exceeded the permissible limit according to the ICNIRP standard and that of the Brussels-Capital Region, on the other hand 9 values (18%) were greater than or equal to the limit imposed by the Salzburg recommendation.

An analysis of these values according to the location of the measurements reveals other realities, namely:

- The average of outdoor measurements is significantly higher than that of indoor measurements (248.23%);

- The average of external measurements exceeds the permissible limit of the Salzburg recommendation;

The average of the internal measurements remains low (44.59%) compared to the most rigorous of the three standards.

Figures 18-20 respectively present the 2D graph of the electric field residuals, its 2D spatial distribution, and its 2D probability distribution for external measurements. Figure 19 shows the residuals, which represent the difference between the observed values and the values predicted by the model. The random dispersion of points around the zero line confirms the linearity of the model; points located on this line correspond to zero residuals. The evolution of the electric field is correlated with Figure 8 from the simulation, showing a gradual increase. Figure 20 assesses the normality of the dataset: the alignment of points indicates a distribution close to normal, which suggests a good fit for the model.

Figures 21-23 illustrate the 2D graphs of the aforementioned parameters for internal measurements. The residual plot in Figure 21 quantifies the model's prediction error, that is, the difference between the experimental data and the simulated values. The random distribution of points on either side of the x-axis confirms the linearity assumption, with zero errors for points aligned with this axis. Regarding the field behavior, Figure 22 highlights a concordance with the simulation results in Figure 9: the resulting profile exhibits sawtooth oscillations superimposed on an increasing trend. Figure 23 serves to verify the normality assumption of the residuals. The near-linearity of the point cloud on this quantile-quantile diagram indicates a satisfactory fit between the model and the internal measurements.

Thus, we can confirm that the measurement results closely match those of the simulations obtained based on Hertzian dipole theory, as Tables 2-4 show the discrepancies recorded between these two approaches. We observe average discrepancies of 0.4% between the 2D simulation and external measurements, and 1.05% between the 2D simulation and internal measurements. These values are within the margin recommended by the standard (RMSE), and we can therefore confirm that our approaches are validated.

7. Conclusions

This study focused on measuring and evaluating electromagnetic radiation emitted by GSM base station antennas, as well as validating the data using metric methods, in the Gombe district (Golf neighborhood) of Kinshasa, an area characterized by a high density of GSM sites. The results demonstrate the absence of specific national standards for non-ionizing radiation (NIR) in the Democratic Republic of the Congo.

The measured levels, with an average electric field of 0.4538 V/m and a power density of 0.1252 W/m^2, are generally below the limits set by the ICNIRP standard, but remain above more restrictive recommendations, such as those of Salzburg. Metric analysis of the data reveals a low measurement error, confirming the reli-

ability and consistency of the experimental results.

Although exposure levels comply with international standards, the application of prevention and precautionary principles remains necessary. Recommendations are made, including optimizing transmission power according to the ALARA principle, properly positioning antennas, and taking sensitive areas into account.

Finally, this study opens up research perspectives focusing on improving measurement systems, refining electromagnetic models and extending analyses to indoor environments, in order to better characterize electromagnetic exposure in dense urban environments.

Conflicts of Interest

The authors declare no conflicts of interest regarding the publication of this paper.

References

[1] Nzao, A.B.S. (2021) Study and Modeling of Human Biological Tissue Exposed to High Frequency Electromagnetic Waves. *Open Journal of Applied Sciences*, **11**, 1109-1121. https://doi.org/10.4236/ojapps.2021.1110083

[2] Nzao, A.B.S. (2022) Analysis and FDTD Modeling of the Influences of Microwave Electromagnetic Waves on Human Biological Systems. *Open Journal of Applied Sciences*, **12**, 912-929. https://doi.org/10.4236/ojapps.2022.126063

[3] Nzao, A.B.S. (2022) Analysis, Sources and Study of the Biological Consequences of Electromagnetic Pollution. *Open Journal of Applied Sciences*, **12**, 2096-2123. https://doi.org/10.4236/ojapps.2022.1212145

[4] ANFR (2017) Protocol for Measuring Exposure Levels to Electromagnetic Fields. This Document from the National Frequency Agency Is the Practical Reference for *In-Situ* Measurements in Urban Areas. https://www.anfr.fr/fileadmin/mediatheque/documents/expace/2017-08-28__Protocole_de_mesure_V4.pdf

[5] Werner, R., Knipe, P. and Iskra, S. (2019) A Comparison between Measured and Computed Assessments of the RF Exposure Compliance Boundary of an *In-Situ* Radio Base Station Massive MIMO Antenna. *IEEE Access*, **7**, 170682-170689. https://doi.org/10.1109/access.2019.2955715

[6] Wessapan, T. and Rattanadecho, P. (2014) Influence of Ambient Temperature on Heat Transfer in the Human Eye during Exposure to Electromagnetic Fields at 900 MHz. *International Journal of Heat and Mass Transfer*, **70**, 378-388. https://doi.org/10.1016/j.ijheatmasstransfer.2013.11.009

[7] Wu, H., Wang, D., Shu, Z., Zhou, H., Zuo, H., Wang, S., *et al.* (2012) Cytokines Produced by Microwave-Radiated Sertoli Cells Interfere with Spermatogenesis in Rat Testis. *Andrologia*, **44**, 590-599. https://doi.org/10.1111/j.1439-0272.2011.01232.x

[8] Li, X.H., *et al.* (2010) Millimeter Wave Treatment Inhibits NO-Induced Apoptosis of Chondrocytes through the p38MAPK Pathway. *International Journal of Molecular Medicine*, **25**, 393-399. https://doi.org/10.3892/ijmm_00000357

[9] Wu, T., Rappaport, T.S. and Collins, C.M. (2015) The Human Body and Millimeter-Wave Wireless Communication Systems: Interactions and Implications. 2015 *IEEE International Conference on Communications* (*ICC*), London, 8-12 June 2015, 2423-2429. https://doi.org/10.1109/icc.2015.7248688

[10] Xia, L., Luo, Q., Lin, H., Zhang, J., Guo, H. and He, C. (2011) The Effect of Different Treatment Time of Millimeter Wave on Chondrocyte Apoptosis, Caspase-3, Caspase-8, and MMP-13 Expression in Rabbit Surgically Induced Model of Knee Osteoarthritis. *Rheumatology International*, **32**, 2847-2856. https://doi.org/10.1007/s00296-011-2080-y

[11] Xu, B., Zhao, K., Ying, Z., Sjoberg, D., He, W. and He, S. (2019) Analysis of Impacts of Expected RF EMF Exposure Restrictions on Peak EIRP of 5G User Equipment at 28 GHz and 39 GHz Bands. *IEEE Access*, **7**, 20996-21005. https://doi.org/10.1109/access.2019.2897271

[12] Yinhui, P., Hui, G., Lin, L., Xin, A. and Qinyou, T. (2019) Effect of Cell Phone Radiation on Neutrophil of Mice. *International Journal of Radiation Biology*, **95**, 1178-1184. https://doi.org/10.1080/09553002.2019.1607605

[13] Zhadobov, M., Alekseev, S.I., Le Dréan, Y., Sauleau, R. and Fesenko, E.E. (2015) Millimeter Waves as a Source of Selective Heating of Skin. *Bioelectromagnetics*, **36**, 464-475. https://doi.org/10.1002/bem.21929

[14] Zhadobov, M., Alekseev, S.I., Sauleau, R., Le Page, Y., Le Dréan, Y. and Fesenko, E.E. (2017) Microscale Temperature and SAR Measurements in Cell Monolayer Models Exposed to Millimeter Waves. *Bioelectromagnetics*, **38**, 11-21. https://doi.org/10.1002/bem.21999

[15] Zhadobov, M., Sauleau, R., Augustine, R., Le Quément, C., Le Dréan, Y. and Thouroude, D. (2012) Near-Field Dosimetry for *in Vitro* Exposure of Human Cells at 60 GHz. *Bioelectromagnetics*, **33**, 55-64. https://doi.org/10.1002/bem.20685

[16] Zhang, Y. (2019). Design and Implementation of 28 GHz Phased Array Antenna System. 2019 *IEEE MTT-S International Wireless Symposium* (*IWS*), Guangzhou, 19-22 May 2019, 1-3. https://doi.org/10.1109/ieee-iws.2019.8804044

[17] Zhang, Y., Ding, J., Duan, W. and Fan, W. (2005) Influence of Pulsed Electromagnetic Field with Different Pulse Duty Cycles on Neurite Outgrowth in PC12 Rat Pheochromocytoma Cells. *Bioelectromagnetics*, **26**, 406-411. https://doi.org/10.1002/bem.20116

[18] Zhang, Y.-W., Yao, Q., Xu, S.-C., Yu, Z.-P. and Zhang, G.-B. (2013) Effects of Acute Millimeter Wave Exposure on the Expression of Substance P and c-fos in Rat Spinal Cord. *Medical Journal of Chinese People's Liberation Army*, **38**, 329-333.

[19] Lin, J.C. and Wang, Z. (2007) Hearing of Microwave Pulses by Humans and Animals: Effects, Mechanism, and Thresholds. *Health Physics*, **92**, 621-628. https://doi.org/10.1097/01.hp.0000250644.84530.e2

[20] Zhao, J.X., Zhao, S.G. and Sun, W.R. (2006) SAR Evaluation in the 0.25 mm Human Eye Model Exposed to 30 GHz Millimeter Wave. *International Journal of Infrared and Millimeter Waves*, **27**, 293-300. https://doi.org/10.1007/s10762-006-9064-0

[21] Stenane, N.M. and Folly, K.A. (2014) Application of Evolutionary Algorithm for Optimal Directional Overcurrent Relay Coordination. *Journal of Computer and Communications*, **2**, 103-111. https://doi.org/10.4236/jcc.2014.29014

[22] Ouattara, S., Loum, G.L., Adama, K. and Clément, A. (2011) Study of a Kit of GSM Radio Operator Site for Event-Driven Movable Coverage: Application to the Deployment of a Site of the Orange Operator in Ivory Coast. *International Journal of Communications*, *Network and System Sciences*, **4**, 744-755. https://doi.org/10.4236/ijcns.2011.411092

[23] Pahalson, C.A.D., Habila, N. and Gaga, H.M. (2024) Array (Smart) Antennas Improve GSM Performance. *International Journal of Communications*, *Network and System Sciences*, **17**, 1-10. https://doi.org/10.4236/ijcns.2024.171001

[24] Xiong, J., Ma, D., Liu, C. and Wang, X. (2013) Secure Communications for Two-Way Relay Networks via Relay Chatting. *Communications and Network*, **5**, 42-47. https://doi.org/10.4236/cn.2013.53b2009

[25] Kamide, N. (2013) A Comparison of Paraconsistent Description Logics. *International Journal of Intelligence Science*, **3**, 99-109. https://doi.org/10.4236/ijis.2013.32011

[26] Wu, H. (2017) The Improvement of Relay Selection Schemes in Two-Hop Cellular Networks. *International Journal of Communications, Network and System Sciences*, **10**, 98-107. https://doi.org/10.4236/ijcns.2017.108b011

[27] Bahrami, H.R. and Le-Ngoc, T. (2010) Maximum Ratio Combining Precoding for Multi-Antenna Relay Systems. *Communications and Network*, **2**, 97-103. https://doi.org/10.4236/cn.2010.22016

[28] Al Islam, A.B.M.A., Hossain, M.S. and Raghunathan, V. (2012) Dynamic Clustering with Relay Nodes (DCRN): A Clustering Technique to Maximize Stability in Wireless Sensor Networks with Relay Nodes. *International Journal of Communications, Network and System Sciences*, **5**, 368-385. https://doi.org/10.4236/ijcns.2012.56047

[29] Lapalorcia, L.M., Abenavoli, F.M. and Cordellini, M. (2011) Double Chondrocutaneous Composite Free Graft in Nasal Reconstruction. Report of a Case and Technique Description. *Surgical Science*, **2**, 481-484. https://doi.org/10.4236/ss.2011.210105

[30] Spaans, A.J. and Beumer, A. (2013) Carpal Coalitions; Failures of Differentiation of the Carpus: A Description of Cases. *Open Journal of Radiology*, **3**, 1-6. https://doi.org/10.4236/ojrad.2013.31001

[31] Ghadimi, S. and Hussian, J. (2012) Effect of Impulse Noise on Wireless Relay Channel. *Wireless Sensor Network*, **4**, 167-172. https://doi.org/10.4236/wsn.2012.46024

[32] Sacchettoni, S.A., Bolaños, J., Torres, N., Abud, J.P., Mantilla, P., Salazar, L., *et al.* (2021) Effects of Microselective Neurotomy on Focal Spasticity and Description of the Surgical Technique. *Open Journal of Modern Neurosurgery*, **11**, 144-156. https://doi.org/10.4236/ojmn.2021.113018

[33] Jing, L., Xu, X. and Wang, Y. (2013) Analysis of Relay Deployment Based on Handover Outage Probability in High Speed Scenarios. *Communications and Network*, **5**, 344-347. https://doi.org/10.4236/cn.2013.53b2063

[34] Hermann, Y.K.J., Phillipe, K.Z., Nabollé, R.G. and Frederic, O.T. (2026) Design of a Security System to Monitor Equipment Performance, Diagnose Anomalies, Predict Failures, and Optimize Operations in Isolated GSM Sites through Sensor Technology: Case of GSM Sites in Burkina Faso. *Journal of Sensor Technology*, **16**, 1-12. https://doi.org/10.4236/jst.2026.161001

[35] Sizykh, V.N., *et al.* (2021) The Automated System of Unified Templates as an Element of Trainability of Microprocessor Relay Protection Devices. *Journal of Applied Mathematics and Physics*, **9**, 3045-3057.

[36] Del Ser, J. and Khalaj, B.H. (2009) Performance Analysis of a Novel Dual-Frequency Multiple Access Relay Transmission Scheme. *International Journal of Communications, Network and System Sciences*, **2**, 592-599.

[37] Venkataraman, H., Kumar Jain, P. and Revanth, S. (2009) Optimal Positions of Relay Stations for Cluster-Based Two-Hop Cellular Network. *International Journal of Communications, Network and System Sciences*, **2**, 283-292. https://doi.org/10.4236/ijcns.2009.24031

[38] Al-Shami, H., Salah, A.M. and Ali, M.F.A. (2020) Double J Fixation after Craniotomy: Technical Description of a Modification Method for Bone Flap Fixation (Hiederov Method). *Open Journal of Modern Neurosurgery*, **10**, 318-324. https://doi.org/10.4236/ojmn.2020.103034

[39] Falahati, A. and Attar Izi, Y. (2012) Employing Power Allocation to Enhance Zero Forcing Scheme Advantages over Multi-Antenna Multiple Relay Networks. *International Journal of Communications, Network and System Sciences*, **5**, 736-742. https://doi.org/10.4236/ijcns.2012.511077

[40] Wang, S., Cui, K. and Huang, Z. (2017) Performance Analysis of an Adaptive Incremental Cooperative Relaying Scheme for Wireless Relay Networks. *International Journal of Communications, Network and System Sciences*, **10**, 48-57. https://doi.org/10.4236/ijcns.2017.108b006

[41] Hasan, R., *et al.* (2015) Microcontroller Based Home Security System with GSM Technology. *Open Journal of Safety Science and Technology*, **5**, 55-62.

[42] Hossain, M.A. and Alam, M.S. (2018) Performance Evaluation of Rectangular Microstrip Patch Antennas Loaded with Plastic and Barium-Titanate Substrates at GSM 1800 MHz Band. *Open Journal of Antennas and Propagation*, **6**, 36-42. https://doi.org/10.4236/ojapr.2018.63004

[43] Yassin, S., Musleh, M. and Abuzerr, S. (2019) Electromagnetic Radiation Exposure from Nearby Cellular Base Stations in the Gaza Strip, Palestine: A Concern for Public Health. *Journal of Biosciences and Medicines*, **7**, 46-59. https://doi.org/10.4236/jbm.2019.74006

[44] Essiben, J.-F.D., Hedin, E.R. and Joe, Y.S. (2010) Radiation Characteristics of Antennas on the Reactive Impedance Surface of a Circular Cylinder Providing Reduced Coupling. *Journal of Electromagnetic Analysis and Applications*, **2**, 195-204.

[45] Nzao, A.B.S. (2023) Analysis and Simulation of the Influence of Electromagnetic Fields on Living Beings near HV Power Lines Using the FDTD Method. *Open Journal of Applied Sciences*, **13**, 2343-2359. https://doi.org/10.4236/ojapps.2023.1312183

[46] Nzao, A.B.S. (2025) Analysis of the Modeling and Biological Consequences of the Electrical Activity of the Human Brain Subjected to 5G Electromagnetic Waves Using Maxwell's Equations. *Open Journal of Applied Sciences*, **15**, 2932-2953. https://doi.org/10.4236/ojapps.2025.159193

[47] Cooray, V., Cooray, G., Rubinstein, M. and Rachidi, F. (2023) Heuristic Estimation of the Vacuum Energy Density of the Universe: Part I—Analysis Based on Time Domain Electromagnetic Radiation. *Journal of Electromagnetic Analysis and Applications*, **15**, 73-81. https://doi.org/10.4236/jemaa.2023.156006

[48] Cooray, V., Cooray, G., Rubinstein, M. and Rachidi, F. (2024) Heuristic Estimation of the Vacuum Energy Density of the Universe: Part II-Analysis Based on Frequency Domain Electromagnetic Radiation. *Journal of Electromagnetic Analysis and Applications*, **16**, 1-9. https://doi.org/10.4236/jemaa.2024.161001

[49] The FDTD Method for Electromagnetic Simulation. https://www.remcom.com/electromagnetic-simulation-numerical-methods/fdtd-method-simulation-software

[50] Yee, K.S. (1966) Numerical Solution of Initial Boundary Value Problems Involving Maxwell's Equations in Isotropic Media. *IEEE Transactions on Antennas and Propagation*, **14**, 302-307. https://doi.org/10.1109/tap.1966.1138693

[51] Schneider, J.B. (2010) Understanding the Finite-Difference Time-Domain Method. https://www.eecs.wsu.edu/~schneidj/ufdtd

[52] Iwata, S. and Kitamura, T. (2011) Three Dimensional FDTD Analysis of Near-Field Optical Disk. *Progress in Electromagnetics Research Symposium Proceedings*, Marrakesh, 20-23 March 2011, 157-160.

[53] Lu, Q., Guo, W., Byrne, D.C. and Donegan, J.F. (2010) Compact 2-D FDTD Method

Combined with Padé Approximation Transform for Leaky Mode Analysis. *Journal of Lightwave Technology*, **28**, 1638-1645. https://doi.org/10.1109/jlt.2010.2048011

[54] Dib, N. and Katehi, L. (1993) Dispersion Analysis of Multilayer Planar Lines Containing Ferrite Regions Using an Extended 2D-FDTD Method. *Proceedings of IEEE Antennas and Propagation Society International Symposium*, Ann Arbor, 28 June-2 July 1993, 842-845. https://doi.org/10.1109/aps.1993.385217

[55] Chu, Q.X., Zhang, S.F. and Xiong, B. (2002) A Compact 2-D FDTD Algorithm for the Analysis of Nonreciprocal Ferrite Phase Shifters. *Proceedings of the* 3*rd IEEE International Conference on Microwave and Millimeter Wave Technology*, Beijing, 17-19 August, 1113-1116.

[56] Macaire, S., Catrain, A., Tortel, S., Joly, J., Girard, S., Bonnet, P., *et al.* (2015) Radiated Ultrashort High-Power Electromagnetic Pulses Induce ATP Release in B16F10 Murine Melanoma Cells. *Journal of Electromagnetic Analysis and Applications*, **7**, 66-74. https://doi.org/10.4236/jemaa.2015.73008

[57] Messaoudi, H., Mourad, A. and Aguili, T. (2016) Electromagnetic Modulation of Dipole Antenna Inside an Infinite Rectangular Waveguide Using MoM-GEC. *Journal of Electromagnetic Analysis and Applications*, **8**, 161-172. https://doi.org/10.4236/jemaa.2016.89016

[58] Pereira, L.P.S. and Terada, M.A.B. (2017) Synthesis of Antennas for Field and Polarization Control. *Journal of Electromagnetic Analysis and Applications*, **9**, 97-112. https://doi.org/10.4236/jemaa.2017.97009

[59] Cooray, V. and Cooray, G. (2017) A Universal Condition Satisfied by the Action of Electromagnetic Radiation Fields. *Journal of Electromagnetic Analysis and Applications*, **9**, 167-182. https://doi.org/10.4236/jemaa.2017.911015

[60] International Agency for Research on Cancer (2013) Monographs on the Evaluation of Radiation Risk to Humans: Non-Ionizing Radiation, Part 2: Radiofrequency Probability Fields. IARC Press.

[61] International Agency for Research on Cancer (2011) IARC Classifies Radiofrequency Electromagnetic Fields as Possibly Carcinogenic to Humans. IARC Press.

[62] World Health Organization (2020) WHO Research Agenda for Radiofrequency Fields. https://www.who.int/publications/i/item/who-research-agenda-for-radiofrequency-fields

[63] Bao, J. and Hu, Y. (2016) Health Effects of Radio-Frequency Electromagnetic Field. *High Voltage Technology*, **42**, 2465-2478. (In Chinese)

[64] World Health Organization (2020) Framework for Developing Health-Based EMF Standards. https://www.who.int/publications/i/item/9241594330

[65] Zheng, X., Bao, J. and Zhu, C. (2014) Robustness of Cell System under Electro-Magnetic Field Disturbance. *High Voltage Technology*, **40**, 3837-3845. (In Chinese)

[66] Wang, Q., Su, H., Bao, J., *et al.* (2013) Primary Reaction for the Environmental Electric and Magnetic Field Exposure around High Voltage Transmission Line on Health Effects. *High Voltage Technology*, **39**, 193-200. (In Chinese)

[67] Liakouti, A. (2018) Analysis and Modeling of Electromagnetic Radiation in PLC Networks. Joint PhD Thesis, Sidi Mohammed Ben Abdellah University of Engineering Sciences and Techniques. https://toubkal.imist.ma/handle/123456789/11105#:~:text=Title:%20Analyse%20et%20mod%C3%A9lisation%20du%20rayonnement%20%C3%A9lectromagn%C3%A9tique,ou%20la%20domotique%2C%20est%20certes%20tr%C3%A8s%20attractif

[68] Joe, Y.S., *et al.* (2012) Design and Modeling of Electromagnetic Impedance Surfaces to Reduce Coupling between Antennas. *Wireless Engineering and Technology*, **3**, 152-159.

[69] Narinyan, L. and Ayrapetyan, S. (2019) Age-Dependent Comparative Study of 4 Hz and 8 Hz EMF Exposure on Heart Muscle Tissue Hydration of Rats. *Open Journal of Biophysics*, **9**, 70-82. https://doi.org/10.4236/ojbiphy.2019.91005